FABRICATION AND CHARACTERIZATION OF CHITIN-CARBON NANOTUBES COMPOSITES

By
Sujeily Soto-Medina
A thesis submitted in partial fulfillment of the requirements for the degree of

MASTER OF SCIENCE
in
MECHANICAL ENGINEERING
UNIVERSITY OF PUERTO RICO
MAYAGUEZ CAMPUS
2015

Approved by:

O. Marcelo Suárez, Ph.D. President, Graduate Committee	Date
Pedro Quintero, Ph.D. Member, Graduate Committee	Date
Ricky Valentín, Ph.D. Member, Graduate Committee	Date
Ricky Valentín, Ph.D. Chair, Mechanical Engineering Department	Date
Agnes Padovani, Ph. D Representative of Graduate Studies	Date

Abstract

Most polymers by themselves have limitations due to their poor mechanical, thermal and electrical properties compared with metallic and ceramic materials. Therefore, to expand their range of applications these properties must be enhanced. In particular, polymer matrix composites are attractive because of their low cost, high tensile strength, high stiffness, and good corrosion resistance. The present study focuses on the fabrication of low cost chitin films reinforced with multiwall carbon nanotubes (CNTs). An additional benefit of this composite is that more than 90% of its mass is biodegradable, which makes it desirable for environmental issues. This composite has potential usage as aerospace structural parts and components. To fabricate these composites, CNTs were dispersed and incorporated into the chitin solution. Different dispersion methods were tested, including ball milling, ultrasonic bath and an ultrasonic probe. The films were characterized with FTIR, optical microscopy, thermogravimetry, and thermomechanical analysis. Better dispersions were obtained via dispersion of the CNT with an ultrasonic bath. The results suggested that the reinforcement effect of the matrix only occurs at high temperature, i.e. 150ºC. At this temperature the polymer is in its rubbery state, which allowed the CNTs to enter in the free volume of the matrix space restraining the movement.

Resumen

La mayoría de los polímeros por sí mismos tienen limitaciones debido a sus pobres propiedades mecánicas, térmicas y eléctricas en comparación con los materiales metálicos y cerámicos. Por lo tanto, para ampliar la cantidad de aplicaciones de materiales poliméricos estas propiedades deben ser mejoradas. En particular compuestos de matriz polimérica son atractivos debido a su bajo costo, alta resistencia a la tracción, alta rigidez, y una buena resistencia a la corrosión. El presente estudio se centra en la fabricación de películas de quitina reforzadas con nanotubos multicapa de carbono. Este compuesto tiene potencial de aplicaciones estructurales y aeroespaciales. Un beneficio adicional de este compuesto es que más del 90% de este material es biodegradable, lo que hace deseable por su poco impacto ambiental. Para fabricar estos compuestos, los CNT se incorporan en la solución de quitina se dispersaron. Diferentes métodos de dispersión se probaron, incluyendo un molino de bolas, un baño ultrasónico y una sonda ultrasónica. Las películas se caracterizaron utilizando FTIR, microscopía óptica, termogravimetría, y el análisis termomecánico. Los resultados mostraron mejores dispersiones cuando el baño ultrasónico se utilizó como método de dispersión de los CNTs en la matrix. Los resultados sugirieron que el efecto de refuerzo de la matriz sólo se produce a alta temperatura, es decir, a 150ºC. A esta temperatura el polímero está en su estado gomoso que permitió a los nanotubos de carbono entrar en el espacio de volumen libre de la matrix restringiendo movimiento de las cadenas.

Acknowledgements

I'm thankful to my advisor, Marcelo Suárez, for giving me the opportunity to work at the Nanotechnology Center and for his direction and support throughout my research.

I would also like to thank to my friends and coworkers at the Materials Research Lab: Boris Renteria, Carlos Rivera, David Florían, Omar Movil, Sugeily Flores, Wesley Cuadrado, Ulises Barajas for their support and cooperation in my research. I'm thankful to my undergraduate students: Deborah Marty, Katiria Esquilin, Jose Salcedo, Christian Rivera, Kiara Rivera and Manny de Jesus.

I would like to thank my boyfriend Hector M. Montalvo for his support and patience.

Finally I would like to thank the Puerto Rico Space Grant Consortium scholarship program and the National Science Foundation for its support under Grant HRD 0833112 (CREST program): Nanotechnology Center for Biomedical and Energy-Driven Systems and Applications and.

Table of Contents

List of Figures

List of Tables

Acronyms and Abbreviations Used in the Research

Some terms have been coined to explain process in the present research. The following list explains the expansions of some of the most commonly used acronyms:

Carbon nanotubes	CNT
Chitosan-starch	CS-ST
Polymer matrix composites	PMC
Glass transition temperature	T_g
Differential scanning calorimetry	DSC
Thermomechanical analysis	TMA
Thermogravimetric analysis	TGA
Degradation temperature	T_d
Simultaneous differential thermal analysis	SDTA
Fourier transform infrared	FTIR
Film made of bare chitin	Ch
Chitin films with CNT treated using HCl and HNO_3.	HCl
Chitin films with CNT treated using acetic acid.	AA
Chitin films with CNT as supplied by Sigma Aldrich.	CNT

1. Introduction

The present study focuses on the fabrication of chitin films, i.e. β-1,4-linked N-acetylglucosamine, $(C_8H_{13}O_5N)_n$, reinforced with multiwalled carbon nanotubes (CNT). Chitin is a natural long chain polymer and one of the most important and abundant in the world. In addition, chitin is very attractive because of its low cost, since it can be obtained from crustacean industry waste [1]. It has a wide range of applications in the medical, pharmaceutical food, cosmetic, and textile industries due to its biocompatibility, biodegradability, and antimicrobial properties [2]. Unfortunately, like most biopolymers, chitin bears poor mechanical and electrical properties that limit its applications. Therefore, the use of CNT as reinforcement can transform this already attractive polymer into a suitable material for further applications in the transportation and aerospace industries.

1.1 Literature Review

1.1.1 Natural Polymer Films

Among the benefits of using biopolymers there is their rapid degradation after disposal when compared to synthetic polymers. The most common technique to fabricate films is based on solvent casting. For instance, chitosan is a pseudonatural polymer deacetylated derivate from chitin [3]. Chitosan-starch (CS-ST) composites films have

potential application in agriculture, food, and pharmaceutical industries. Starch and chitosan films have been produced individually but have limitations due to the water solubility and relatively high water vapor transmission rate, respectively [4]. Y.X. Xu et al. used two types of starch to fabricate CS-ST composites [4]. These composites showed higher tensile strength for starch concentrations up to 50 %. Yet, the addition of starch to chitosan decreased the water transmission in comparison with bare chitosan, making the CS-ST composites better option for food packing in comparison with the bare chitosan. CS-ST films are just one example of the numerous natural polymer films that had been studied with potential biomedical applications in the past years. Sensors are other prospective application for natural polymers films, such as chitin-polyaniline films. These materials showed higher electrical conductivity for larger polyaniline concentrations. This increase in conductivity makes these films suitable for humidity sensor. For the present thesis work, we have fabricated and characterized chitin and chitin cellulose films. CNT were added to the film in order to enhance the mechanical properties of the polymeric matrix.

1.1.2 Natural Polymer-Carbon Nanotube Composites

Since critical polymer matrix composites (PMC) properties depend on the properties of the reinforcement, CNT became the material of choice of many researchers, as they are well known for their great mechanical, electrical and optical properties [5]. The addition of CNT to a PMC has gained popularity because of the low filler to matrix

ratio necessary. This translates into low weight-to-mechanical performance ratios [6]. Automobile bumpers made with 1-5w% CNT have good mechanical properties, enough to be utilized to replace the standard fiberglass bumpers containing 30w% or more of fiberglass [6]. Despite there is no general rule, most polymer carbon nanotubes composites reach their maximum tensile strength when only 1% CNT are added. This is mainly due to poor dispersion when higher concentrations are present [7]. Moreover, resulting mechanical properties of the composites depend highly on the dispersion of the CNT in the matrix. In the scientific literature, there are plenty of procedures to achieve such CNT dispersion. Some of the methods include solution sonication and no fluid high sheer mixing [8]. Particularly, sonication has been used in the fabrication of CNT-chitosan nanocomposites. The dispersion of the CNT was achieved by suspending them in water followed by sonication. The suspension was later added to the polymer solution and sonicated to ensure homogenization [9]. These composites were tested for the removal of heavy metals obtaining up to a 90 percent removal. CNT-polymer nanocomposites have been made by just adding the carbon nanotubes in to the polymer solution dispersing them using a sonicator, and finally completing a solvent casting to obtain random alignment of the CNT. These nanocomposites were also fabricated aligning the nanotubes during the solvent casting between two poles of a magnetic field [10]. A. Sharma et al. found higher gas permeability for CNT-polycarbonate composites magnetically aligned than for those randomly aligned. The CNT-polycarbonate magnetically aligned also showed an increased in electrical conductivity and higher dielectric constant as compared to randomly oriented composites[10]. So far, we have discussed the dispersion of CNT in solution but there are also methods of dispersion by

solid phase. Some studies showed that grinding the CNT decrease the agglomerates[11][12]. Other solid phase technique that had successfully dispersed the CNT is the calendaring [13][14]. The interaction between the matrix and the CNT is also an important factor in the resulting properties of the CNT composites. The functionalization of the CNT had been proved to improve the interaction between the matrix and the CNT [13]. CNT-chitosan composites fabricated by L. Carson et al. showed improved thermal properties of the matrix. These composites were synthesized by functionalizing the CNTs and by covalent integration of the CNT to the matrix [15].

One can observe in the literature that most of the researches that had been working with polymers CNT composites had been using synthetic matrices. Only few attempted to use natural (biodegradable) polymers. At the moment of the writing of this thesis, there have been no accounts available in the literature using α-chitin as the matrix for a novel polymer carbon nanotube composite. For that reason, we believe that the present scientific contribution demonstrates how the presence of CNT in a chitin matrix can positively affect the mechanical strength of the composite particularly at higher temperatures, i.e. 100 and 150ºC, when compared with bare chitin.

1.2 Objectives

Our hypothesis is that chitin films reinforced with CNT will have higher tensile strength, higher stiffness, and high fracture toughness as compared to bare chitin films.

Therefore, to demonstrate that hypothesis, the goals of this thesis are:

1. Optimization of the bare chitin film fabrication process.
2. Fabrication of chitin films reinforced with carbon nanotubes.
3. Extensive mechanical characterization of the CNT composites.
    a. Tensile strength
    b. Young’s modulus
    c. Creep behavior

2. Theoretical Background

2.1 Chitin

Chitin chains are one form of N-acetyl-D-glucosamine. This polymer is the second most abundant polymer in nature with cellulose being the first one. Chitin is naturally synthetized in the exoskeleton of arthropods (shrimp, crawfish, etc.), as a semi-crystalline polymer. The annual production of chitin in nature is estimated around 10^{11} tons [16]. Crustaceans industry generates around 60,000 tons of waste and about 10% of that weight is chitin [17]. Despite the abundance of this polymer, its uses are limited as a result of its low solubility in most common organic solvents. Through the de-acetylation of chitin a derivate called chitosan is obtained. Chitosan can be dissolved by common solvents like acetic and hydrochloric acid, which makes it easier to process than chitin. Despite this advantage, such high solubility can be a drawback for applications where the material could be exposed to harsh conditions.

The strong hydrogen bonds between the layers formed by the polymer chain give chitin structural and chemical stability. The acetyl groups which are present only in the chitin chains are responsible of some of the intramolecular interactions. Nowadays, chitin has applications in the medical, pharmaceutical, food, cosmetic, and textile industry,

mostly due to its biodegradable and antimicrobial characteristics. Additionally, this polymer has been used as reinforcement for other polymers like rubber and PVA [18][19].

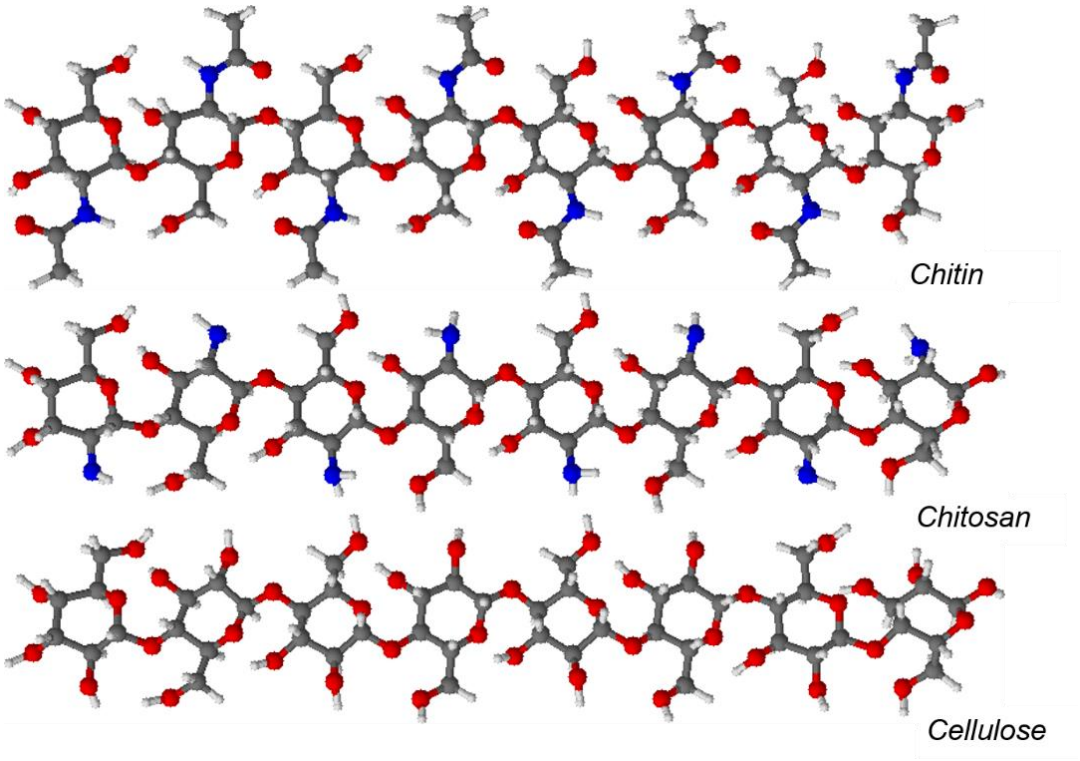

Figure 1. Chemical structure of chitin, chitosan and cellulose.

2.2 Polymer-Carbon Nanotubes Composites

2.2.1 Carbon Nanotubes

Carbon nanotubes possess excellent thermal, mechanical, and electrical properties and, as a consequence, since their discovery they have been the focus of many studies throughout the world. Their diameter can vary from 1 to 100nm and their

Young's modulus has been reported to reach 1 TPa. Their densities have been found to be as low as 1.3 g/cm^3 with a tensile strength up to 200 GPa[20][13]. These outstanding properties have made them especially attractive in the fabrication of composite materials. Depending on the matrix selected, the resulting composite material can have unusual and unique combination of stiffness, strength, weight, corrosion resistance, hardness, and conductivity. They have also been used to produce composites with strong thermal conductivity properties. For instance, researchers have been studying the CNT to find ways to use their conductivity and high aspect ratio to fabricate conductive plastics with very low percolation threshold. The percolation threshold refers to the concentration of the filler network that exhibits long range connectivity [8].

2.2.2 Composites

In a composite material, an appropriate mechanical reinforcement requires four conditions or requirements. These four conditions are: uniform dispersion, high aspect ratio, alignment, and interfacial stress transfer [7] [21]. The one requirement that is always singled out as the fundamental one is the dispersion. It is important to obtain a good dispersion because this allows for a more efficient and productive load transfer to the nanotube network. This further helps the composite obtain a better and more uniform stress distribution. It also reduces the risks of stress concentration points. Bad dispersions usually cause degradation of the mechanical properties of the composites.

Alignment, on the other hand, provides more stiffness and is also important when it comes to improving strength. It has been proven, however, to be more important in fibers because it maximizes reinforcement [22].

When it comes to fabricating a composite material it is imperative that there is a adequate load transfer across the matrix-reinforcement interface. This enables the composite to successfully transfer applied external stresses to the nanotubes network. In doing so, the load is distributed in a disproportional manner throughout the nanotubes thus creating a stronger composite. It is important to note that interfacial shear stress transfer is also considered a great parameter for fiber-composites [23] [7].

2.3 Thermomechanical Analysis

2.3.1 Glass Transition Temperature

It is well known that most polymers are sensible to temperature changes. In particular, the glass transition temperature (T_g) is only exhibited by semicrystalline and amorphous polymers. Above this temperature, the polymer behaves as a viscous liquid depending on its crystallinity and molecular weight. At temperatures below the T_g, the material becomes brittle [24], [25]. Since polymer properties are strongly affected by this temperature, T_g is an important parameter to be studied. This can be performed by

different techniques such as dilatometry, differential scanning calorimetry (DSC), dynamic mechanical analysis (DMA), and thermomechanical analysis (TMA) [26][27]. The T_g may vary with different techniques, especially when comparing the mechanical versus calorimetric techniques. The addition of a filler to the polymer can increase or decrease the chain mobility [28]. This chain mobility change will naturally decrease or increase the T_g respectively. In the present work, a TMA was used to determine the T_g of chitin-CNT films. In the experimental section, a detailed explanation of the calculation to obtain this property will be provided.

2.3.2 Coefficient of Thermal expansion (CTE)

TMA also allows for the calculation of the CTE, which is a measurement of the dimensional changes the material undergoes when temperature is altered. Polymers in general have larger CTE values due to the low activation energy needed to change the configuration [29]. In the fabrication of composite materials consideration of the CTE of its components is mandatory. For instance, a matrix with a CTE lower than the filler CTE can build up internal stresses causing a premature failure of the material [30]. The CTE can be calculated by measuring the free volume space or the strain in a temperature range. The expansion coefficient can be calculated from the linear region of the strain temperature curves obtained from the TMA. An abrupt change in the slope will be an indication of an increase in free volume space and the glass transition temperature. The CTE is normally reported for a temperature range.

2.3.3 Creep

Materials such as polymers, bearing constant stress below their tensile yield strength for a period of time, undergo permanent deformation that will eventually lead to failure. This time-dependent deformation is called creep [31]. It is well known that the creep behavior of most materials can be described by three stages. During the first stage, the material suffers decelerating creep strain rates. The second stage of creep is characterized by a constant strain rate (Figure 2 and Figure 3). During the third and final stage the creep strain rate accelerates leading to the failure of the material.

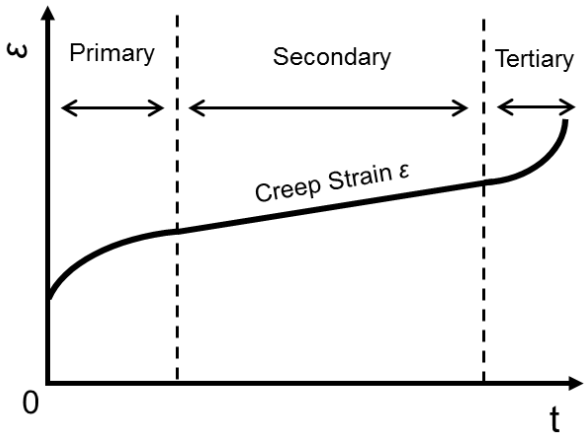

Figure 2. Three stages of creep in a strain vs time curve.

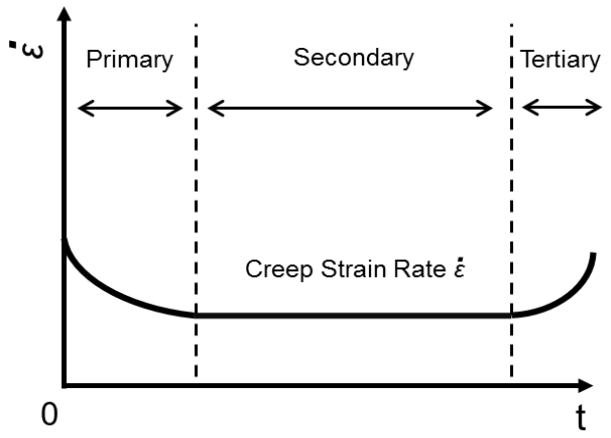

Figure 3. Three stages of creep in a strain rate vs time graph.

For instance, the rate of this deformation for polymer matrix composites (PMC) can be affected by multiple factors: temperature, reinforcement dispersion and interaction with the matrix, and concentration of the dispersed phase [31]. Creep deformation can be due to bond rotation (elastic) and/or links and chains slides (plastic) [32]. As a consequence, creep behavior of these viscoelastic materials can be modelled by a series of dashpot and springs. The dashpot represents the viscous behavior with the spring being the elastic behavior of the material (Figure 4).

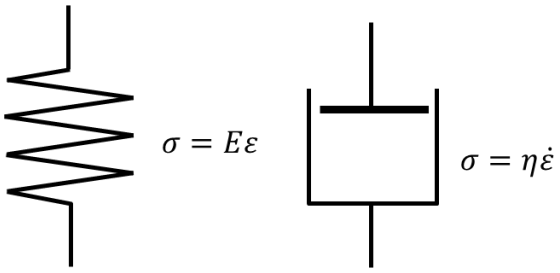

Figure 4. Spring and Dashpot elements.

In particular, the Maxwell model represents the creep strain by a dashpot and spring connected in series while in the Voigt model the dashpot and the spring are arranged in parallel (Figure 5) [33], [34]. As a result, the total strain in the Maxwell model is described by equation 1.

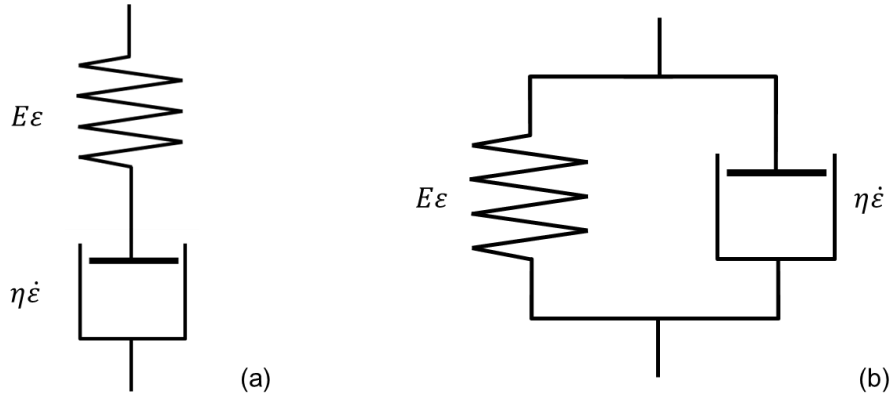

Figure 5. Maxwell (a) and Voigt (b) model representations.

$$\varepsilon = \varepsilon_s + \varepsilon_d \qquad 1$$

Where ε_s and ε_d are the strain of the spring and the dashpot, respectively. By writing ε_s and ε_d in terms of stress, equation 2 is obtained:

$$\varepsilon = \frac{\sigma}{E} + \frac{\sigma}{\eta}t \qquad 2$$

Where σ is the applied stress, η is the coefficient of viscosity t is the time under load and E is the Young's modulus. For the Voigt model, $\varepsilon = \varepsilon_s = \varepsilon_d$ and in terms of stress, the total stress will be the sum of the stress applied to the spring and the stress applied to the dashpot, according to equation 3.

$$\sigma = \sigma_s + \sigma_d \qquad 3$$

In terms of strain-time dependence, equation 3 can be written as equation 4:

$$\varepsilon = \frac{\sigma}{E}\left[1 - exp\left(-\frac{Et}{\eta}\right)\right] \qquad 4$$

The Burgers model (Figure 6) is a combination of the Maxwell and Voigt model which can be expressed by equation 5

$$\varepsilon = \frac{\sigma}{E_1} + \frac{\sigma}{E_2}\left[1 - exp\left(-\frac{E_2 t}{\eta_2}\right)\right] + \frac{\sigma}{\eta_1} t \qquad 5$$

Alternatively, in terms of creep compliance J, the resulting equation 6 is obtained.

$$J = \frac{1}{E_1} + \frac{1}{E_2}\left[1 - exp\left(-\frac{E_2 t}{\eta_2}\right)\right] + \frac{t}{\eta_1} \qquad 6$$

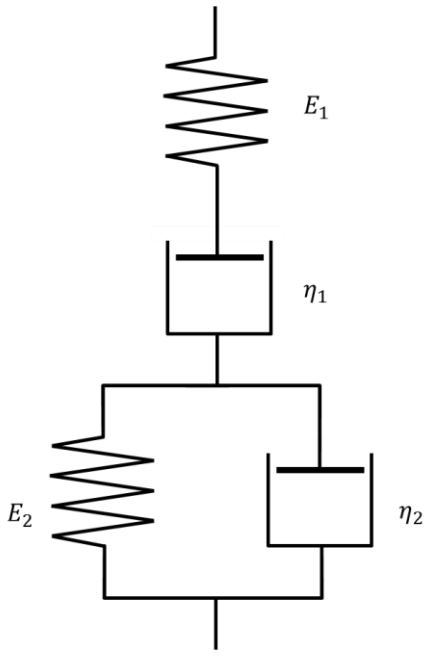

Figure 6.Four elements (Burger) model.

Another approach to model the creep behavior of most materials is using the power law (equation 7), which is a more empirical model. Differing from Maxwell and Voigt models, this one does not take any physical conditions into consideration.

$$J(t) = J_0 + J_1 t^n \qquad 7$$

Where J the compliance, t is the time, n a constant independent of stress, J_0 is the time independent compliance, and J_1 is the coefficient of time-dependent term. By taking the natural logarithm on both sides of equation 7, one can rewrite it as equation 8:

$$\ln(J - J_0) = \ln(J_1) + n\ln(t) \qquad 8$$

As mentioned before, temperature has a significant effect on the creep deformation. In particular, polymers will have higher creep above their T_g. In the study of the temperature effect on the creep behavior, rather than obtaining sets of creep curves for different temperatures using the “time-temperature superposition principle”, a master curve can be prepared. The Williams, Landel and Ferry (WLF) equation is one of the most commonly used to determine the shift factor a_T. This equation will produce the master curve and is defined by equation 9 [35][34][33]:

$$\log(a_T) = \frac{-C_1(T - T_s)}{(C_2 + T - T_s)} \qquad 9$$

where T_S is an arbitrarily selected reference temperature and C_1 and C_2 are material constants.

3. Experimental Procedure

3.1 Materials

The matrix of the nanocomposite was fabricated by dissolving chitin flakes. The chitin flakes were γ-irradiated (200kgy) in order to decrease the molecular weight of the polymer to favor its solubility [36]. The solvent system proved to successfully dissolve chitin was N-N dimethylacetamide (C_4H_3NO 99%) and 5% lithium chloride (LiCl ACS 99%) provided by Alfa Aesar. The CNTs used in this research where provided by Sigma-Aldrich in dry form. MWCNTs synthetized by chemical vapor deposition were selected because of their low cost compared to the SWCNT and other methods of fabrication [20]. These MWCNTs are 5µm long and have an outside diameter of 6 to 9nm. Hereon, we will use CNT to refer to the nanotubes used in our composite.

3.2 Film Synthesis

To fabricate the composite material, i.e. chitin films reinforced with CNTs, the nanotubes were incorporated and dispersed into the chitin solution. The solutions are poured in petri dishes and coagulated using 2-propanol. Finally the coagulated gel are left in the furnace at 60ºC for two days and then dried between two glass plates at room temperature (Figure 7).

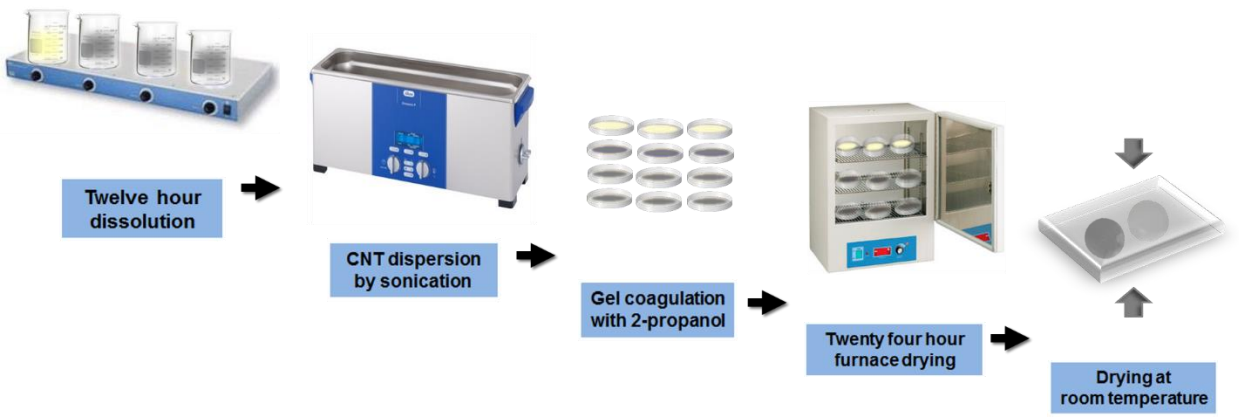

Figure 7. Methodology for the preparation of the chitin-CNT composites

3.3 Carbon Nanotubes Dispersion

The dispersion of the CNTs was completed by sonication of the chitin-nanotube solution, ball milling, or a combination of both techniques.

3.3.1 Ultrasonic Probe

After the preparation of the chitin/CNT solutions they were sonicated using an ultrasonic processor from Cole Palmer.

3.3.2 Ultrasonic Bath

The chitin/CNT solutions were submerged in the ultrasonic bath FS220H from Fisher Scientific for one hour.

3.3.3 Ball Milling

A varioplanetary high energy ball milling helped with the dispersion of the CNT. The high energy ball mill operated at 300rpm and 500rpm was furbished with tungsten carbide grinding balls with 11.2 mm in diameter.

3.4 Carbon Nanotubes Treatment

To enhance the dispersion of the nanotubes into the matrix, they were treated with strong acids. This treatment consists in mixing the CNTs with acetic acid or a solution of hydrochloric and nitric acid. The CNTs were mixed with the acid in a magnetic stirrer for 72 hours and 1 hour of sonication, followed by washing and drying (Figure 8).

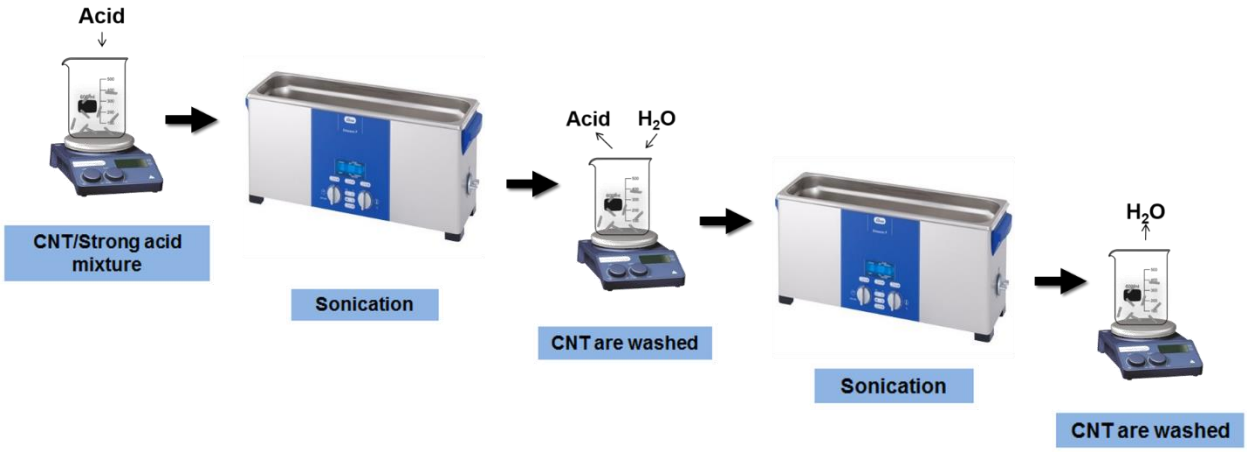

Figure 8. Methodology for the treatment of the CNT.

3.5 Characterization

3.5.1 Optical Microscopy

A Nikon Epishot 200 optical microscope was used to examine the film morphology and to have a closer look of the dispersion of the CNT of the matrix.

3.5.2 Zeta Sizer

A Zetasizer Nano S from Malvern was used to determine the size of the carbon nanotube agglomerates. This apparatus uses dynamic light scattering to measure particle size. The nanotubes analyzed were suspended in 2-propanol.

3.5.3 Nanoindentation

A Nano Indenter G200 by Agilent Technologies was used to study hardness and Young's modulus of the produced materials. The technique employed was the continuous stiffness measurement method [37]. The experiments were carried out using a three-sided diamond pyramid Berkovich tip that penetrates the sample at a strain rate of 0.1 s^{--1} up to 3,000 nm in depth.

3.5.4 Tensile Test

Stress–strain curves of the composite films under tensile mode were obtained using a low-force universal testing machine Model 5944 from Instron. In order to calculate the Young's modulus, a pair of extensometers were used during the runs. The samples tested had a dog bone shape according to ASTM1708.

3.5.5 Differential scanning calorimetry (DSC)

Differential scanning calorimetry was performed using a differential scanning calorimeter DSC TA Q20. The temperature range analyzed was 25° to 500°C at a range of 5°C/min in a nitrogen atmosphere. A first run from 25° to 100°C was performed in order

to remove the moisture of the samples. The T_g as well as the degradation temperature (T_d) were evaluated.

3.5.6 Thermogravimetric analysis (TGA)

Thermogravimetric analysis was performed in order to study the moisture content of the samples. Also the T_d of the composite was determined using a TGA/SDTA from Mettler Toledo. The procedure consisted of a ramp from 25° to 500°C for the composites and 25° to 800°C for the CNT at a heating rate of 5°C/min in a nitrogen atmosphere.

3.5.7 Thermomechanical analysis

Thermomechanical characterization of the composite was carried out using a TMA/SDTA84e from Mettler Toledo. The TMA measures dimensional changes in the films due to change in free molecular volume as a function of temperature, time and an applied force [24]. As discussed before, the study of T_g, CTE and creep behavior of polymeric materials is important due to their sensibility to temperature changes. To assess the T_g and to calculate the CTE the samples were tested with a constant tension load while the temperature increased from 25° to 200°C at a 5°C/min heating rate in a nitrogen atmosphere. The T_g was then measured by the onset point from the step transition during

temperature ramping using the STARe software from Mettler Toledo, as shown in Figure 9.

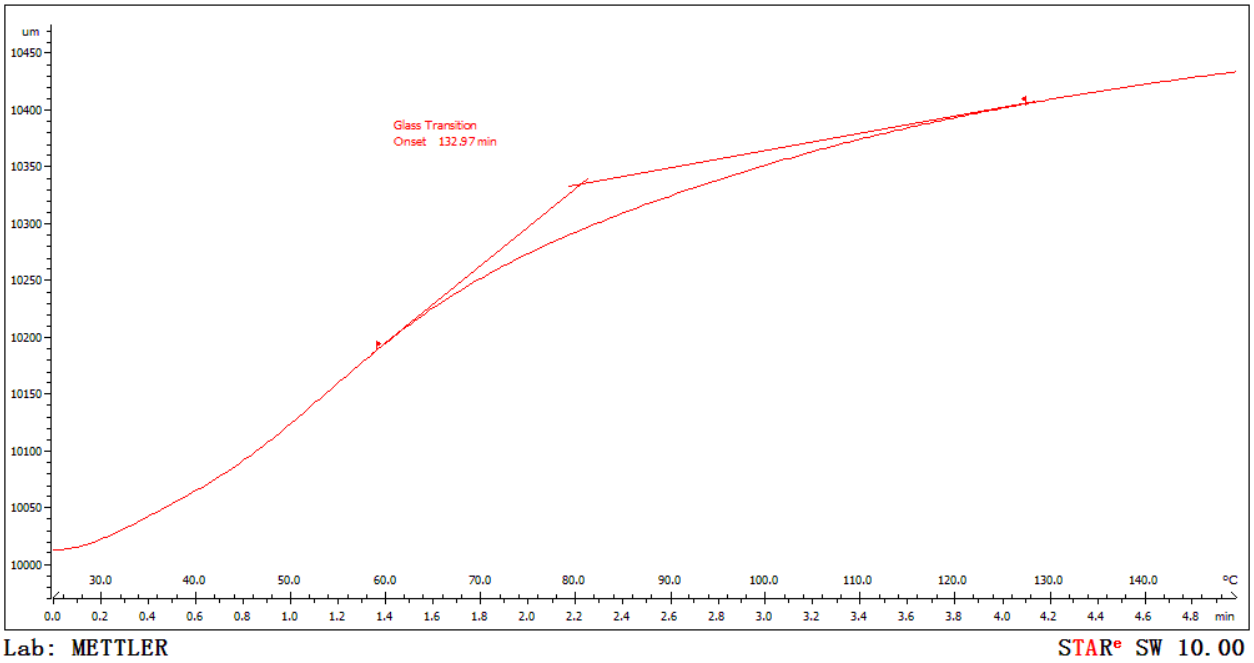

Figure 9. Glass transition temperature calculated using STARe software.

The CTE values reported were calculated using the same software at a temperature range above the glass transition. The TMA also allowed completing creep experiments at four different temperatures. The experiments had a duration of 3 hours where the sample was under a constant tension load and at a constant temperature.

4. Results & Discussion

4.1 Preliminary Results

The optical micrographs in Figure 10 show different chitin-CNT composite samples. Each specimen was prepared using different dispersion methods of the nanotubes. The film made with the CNT powder subjected to a high shear mixing process and then dispersed in the chitin solution via ultrasonic bath showed a better dispersion. After the fabrication process, the films were analyzed with the TMA/SDTA841e differential thermal analyzer. The T_g values of all chitin-CNTs composites with different dispersion methods did not evidence significant changes. The T_g also did not change between the bare chitin film and chitin-CNTs films either. Figure 11 shows two representative curves obtained for bare chitin and chitin-CNTs films. In Figure 11, one can also observe that the sample without CNT underwent more deformation during the T_g experiments.

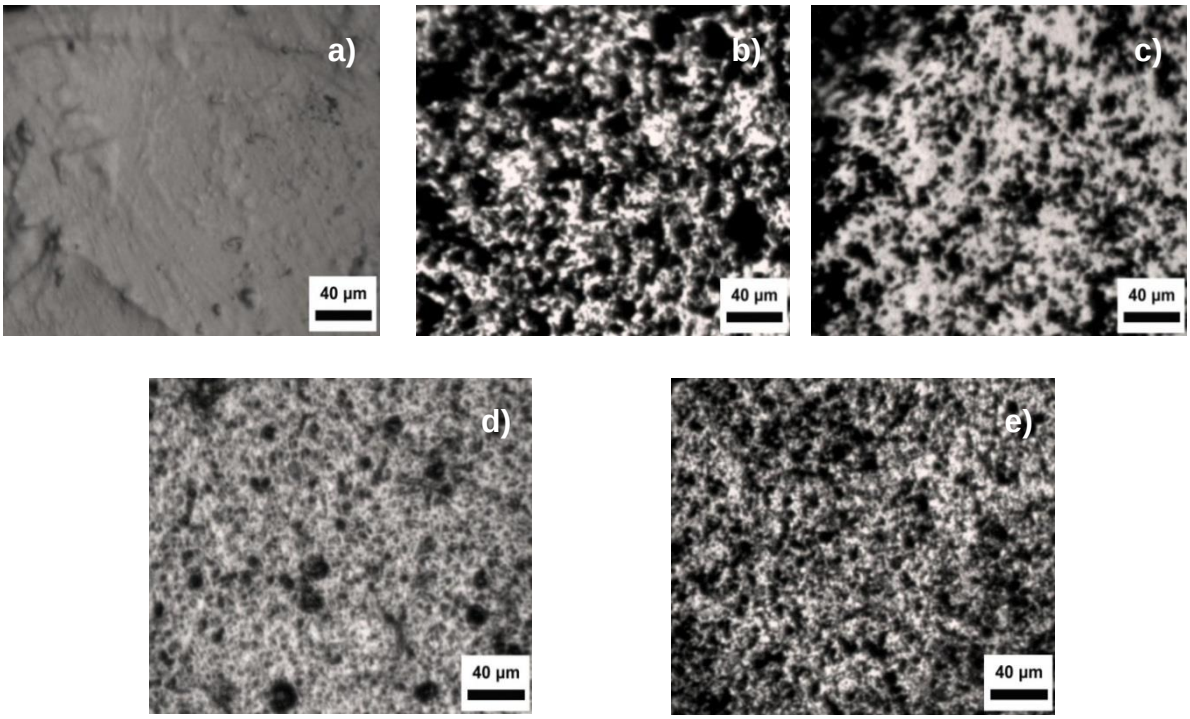

Figure 10. Micrographs of a) bare chitin film, b) chitin-CNTs film using ultrasonic probe as dispersion method, c) chitin-CNTs film using CNTs dispersed in dry form by ball milling, d) and e) chitin-CNTs film using CNTs dispersed in dry form by ball milling at 300 rpm and 500 rpm respectively and later dispersed in the polymer solution by utrasonic bath.

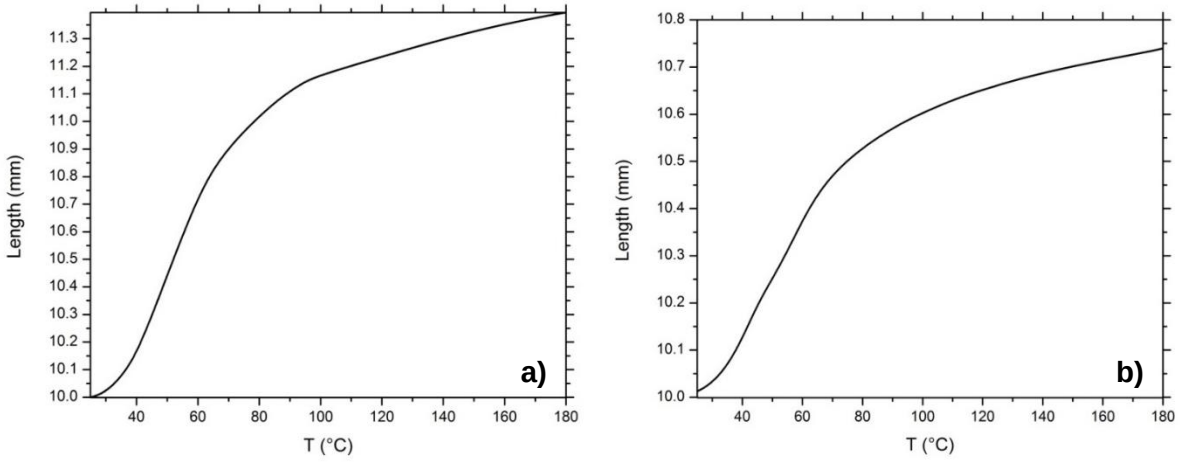

Figure 11. Length change vs temperature plots for a.) bare chitin and b.) chitin-CNTs films.

The graphs in Figure 12 show the strain percent of the chitin-CNTs composites fabricated with different methods of dispersion, subjected to a constant load of 0.5N at 150ºC for three hours. The composites fabricated after dispersing the CNT using ultrasonic probe produced the lower tensile strength (Figure 12a). This may be a consequence of partial polymer decomposition due to high local temperature during dispersion. This lower tensile strength could have also been a product of a poor dispersion of the CNTs. As mentioned before, adequate dispersion is fundamental for the performance of the composites. Our composite is not the exception as we expected that the dispersion is the factor negatively affecting its mechanical properties. On the other hand, using the ball mill to disperse the CNTs powder before dissolution combined with sonication after dissolution of the polymer, resulted in a higher tensile strength (Figure 11 b). A seen before, these composites were also the ones that showed better dispersion. The highest tensile strength was obtained in films with CNTs dispersed in a ball mill at 500rpm and later in solution dispersion by ultrasonic bath. This particular sample showed 85% less deformation in comparison with the bare chitin specimen (Figure 12.c).

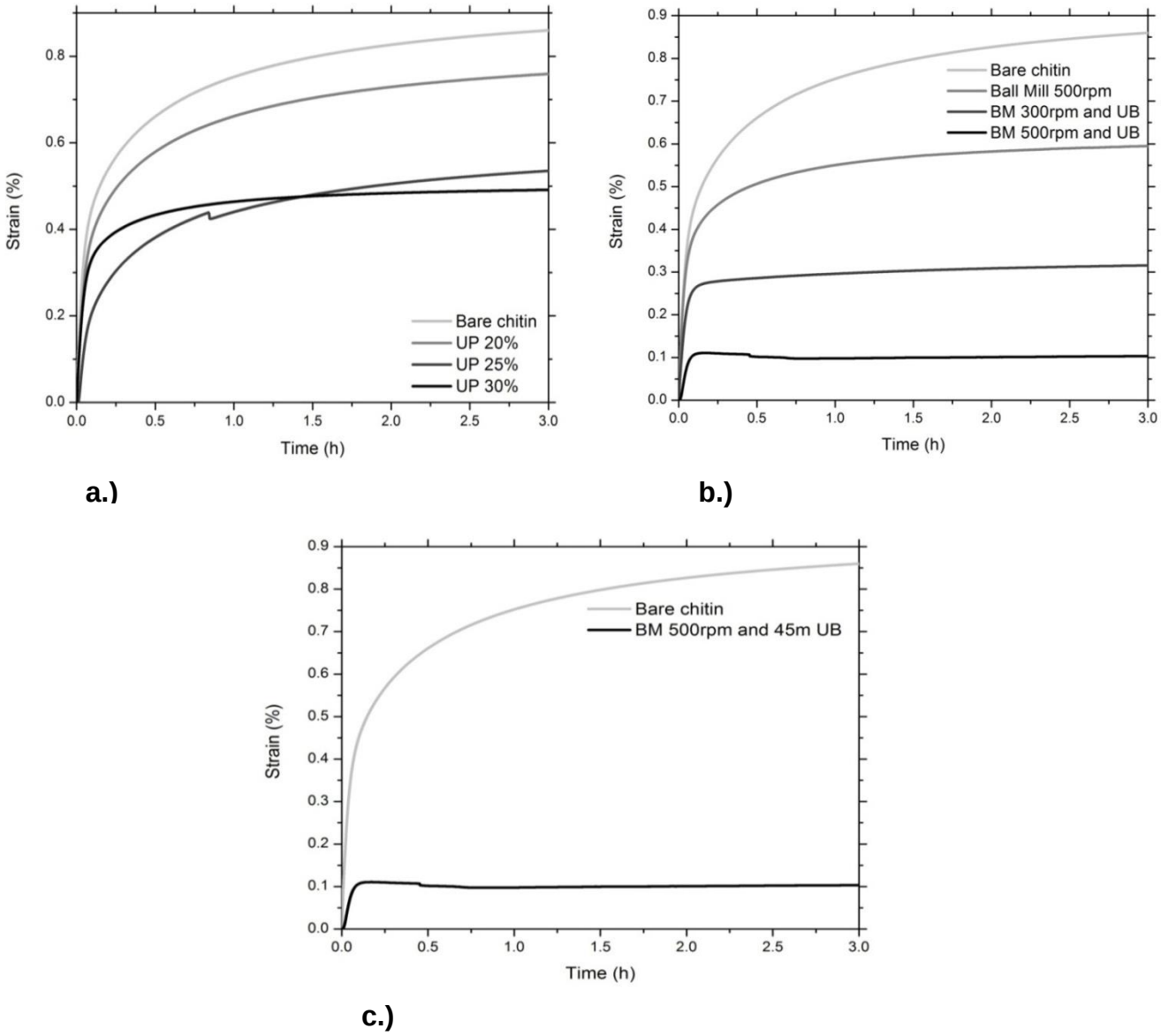

Figure 12 . Strain percent of the chitin-CNTs composites fabricated with different methods of dispersion: a) ultrasonic probe (UP), b.) ball milling and/or ultrasonic bath (UB) and c.) shows the strain percent of bare chitin and the chitin/CNTs film with highest resistance to deformation.

These preliminary results demonstrated that we obtained the best dispersion using the ultrasonic bath to sonicate the polymer solution and the ball milled CNTs. Based on these results, a design of experiments was constructed to determine the best parameters for the dispersion of the CNTs (Table 1). For run order 1, only CNTs were added to the

ball mill jar, while in run order 4, the same weight (amount) of CNTs and chitin were added to the jar.

Standard Order	Run Order	CNT/Chitin w%	Ball milling time (min)
4	1	100/0	60
3	2	100/0	30
1	3	50/50	30
2	4	50/50	60

Table 1 . Experimental design for the dispersion of the CNTs in the composite.

The micrographs in Figure 13 correspond to four samples obtained through the design discussed. Observing the optical micrographs one could infer that there were no significant differences in terms of CNTs dispersion among the four different samples.

The CNTs from run 1 and 2 were suspended in 2-propanol and analyzed using the zeta sizer. The average size of the CNTs after 30 and 60 minutes of ball milling were 2.3 µm and 1.3 µm, respectively.

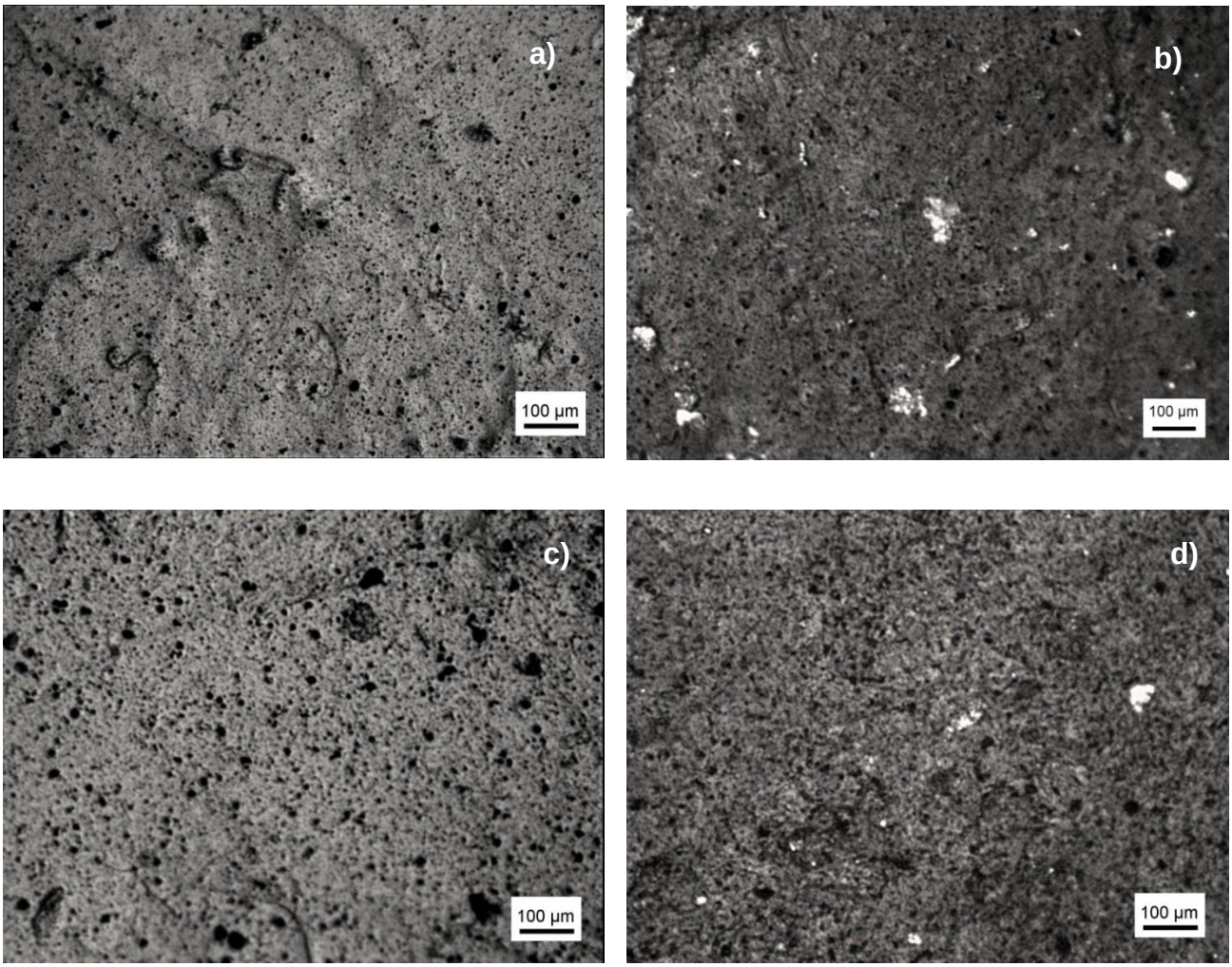

Figure 13 Optical micrographs of the films from run order a) 1 b) 2 c) 3 d) 4.

Nanoindentation experiments to determine the hardness and Young's modulus of the four samples were also completed. Figure 14 shows the measured hardness versus nanoindentation depth curves obtained on bare chitin film and on a representative chitin-CNT film sample. The hardness values were averaged from 25 different sample locations and are summarized in Table 2, where it is apparent that the nanoindentation hardness increased from 0.04 to 0.30GPa. Figure 15 presents curves of Young's modulus versus displacement into surface (depth). These elastic moduli are presented in Table 2 where

the increase of Young's modulus resulting from the addition of CNTs is evident: from 1.2 to 6.2 GPa.

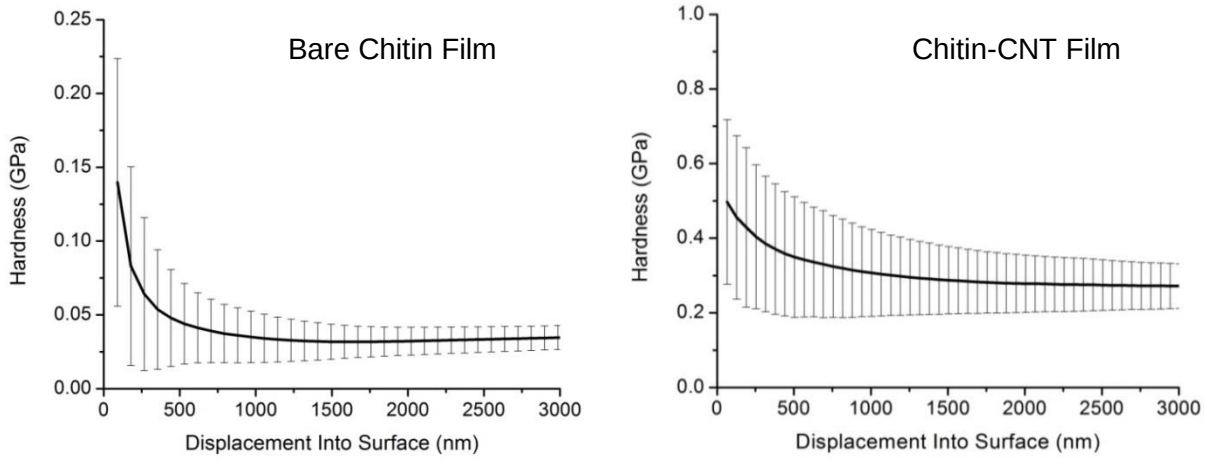

Figure 14. Nanoindentation hardness versus displacement (penetration into the sample).

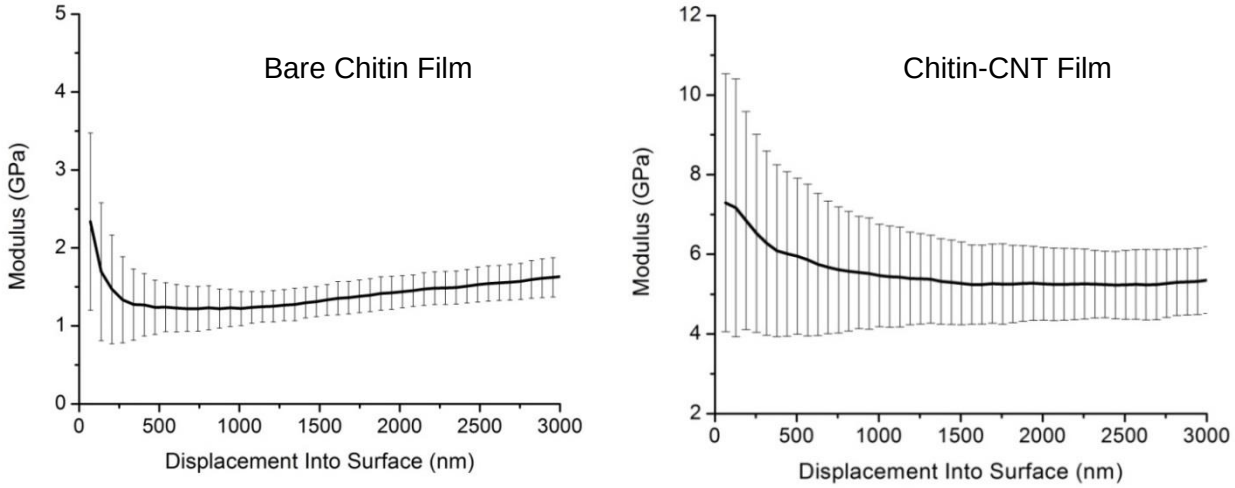

Figure 15. Nanoindentation modulus versus displacement.

Figure 16 shows typical tensile curves of chitin and chitin-CNT films.

In Figure 17 the mean tensile properties in the four chitin-CNTs films and in the pure chitin film are plotted. Higher tensile strength was measured on films with CNTs with no significant difference among runs. These results suggested the enhanced strength of the CNT-reinforced polymeric matrix composites.

Sample	Young's Modulus (GPa)	Standard Deviation	Hardness (GPa)	Standard Deviation
Chitin	1.2	0.2	0.04	0.01
1	6.2	1.7	0.31	0.1
2	5.3	0.4	0.28	0.03
3	5.4	1.4	0.26	0.1
4	5.5	1.2	0.3	0.11

Table 2. Nanoindentation modulus and hardness values for bare chitin and chitin-CNTs run order 1, 2, 3 and 4.

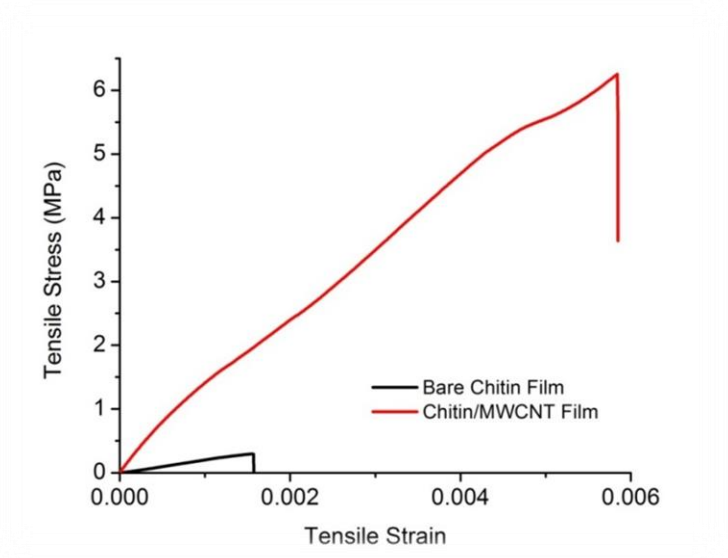

Figure 16. Stress-strain curves of bare chitin and chitin-CNT films.

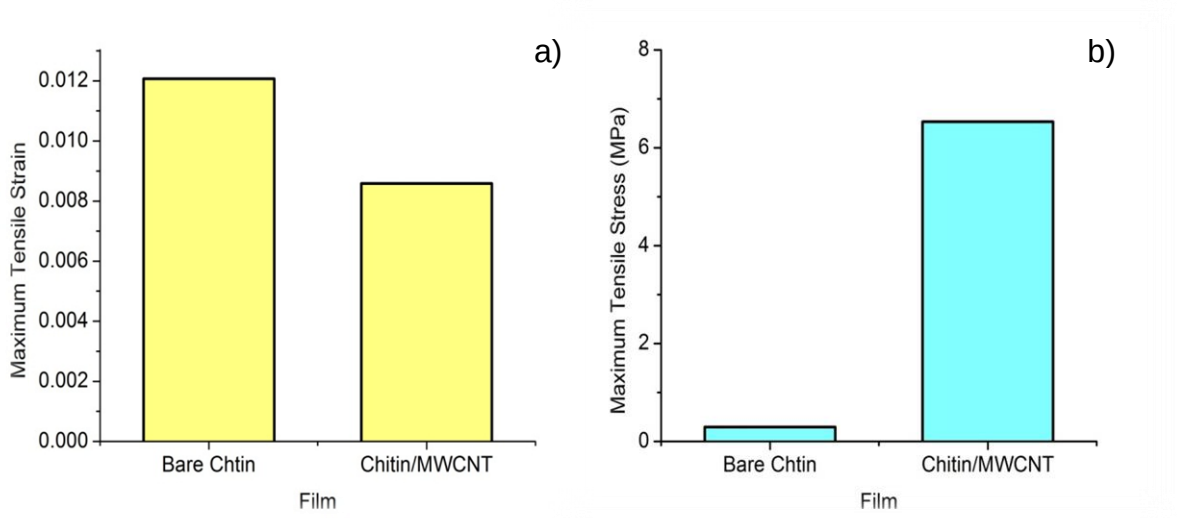

Figure 17. a) Average maximum tensile strain and b) Average maximum tensile stress.

DSC helped determine the glass transition temperature of our PMC after a preliminary heating cycle to dehydrate the film. In this first heating cycle, an endothermic peak caused by dehydration occurred around 70ºC. This value is slightly higher for the films with CNTs. The second DSC cycle (Figure 18) displayed a smooth endothermic step around 95ºC that can be due to the glass transition. The T_g values for the chitin-CNTs films showed no significant change among different dispersion methods. There were also no significant difference between the T_g values for the bare chitin and the chitin-CNTs films.

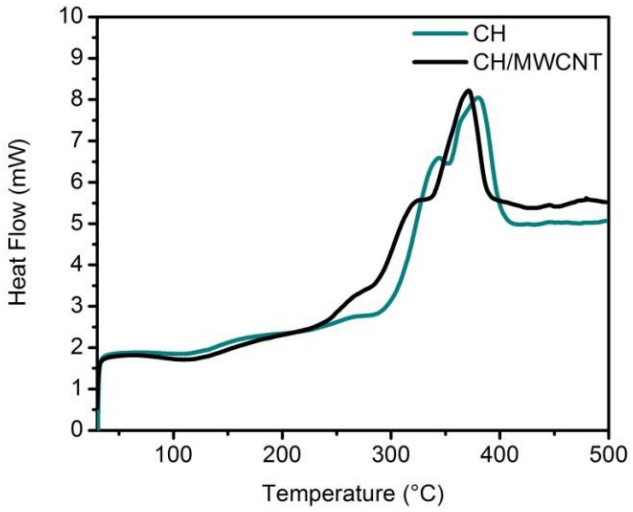

Figure 18. DSC heat flow curves for bare chitin and one of the composite.

After the preliminary results, we decided to fabricate four different samples. A film made of bare chitin (Ch) and the other three with 1w%CNT. The nanotubes used in these composites were as bought (CNT), treated with acetic acid (AA) and the third ones used were treated with a mixture of hydrochloric acid and nitric acid (HCl).

4.2 Optical Microscopy

Figure 10 shows the optical micrographs of the Ch, CNT, HCl and AA nanocomposites. As aforementioned, each specimen was prepared adding CNT as-provided as well as CNT with different acid treatments to the polymer solution. Observing

the optical micrographs one could infer that the films made with the CNT treated with acids achieved better dispersion.

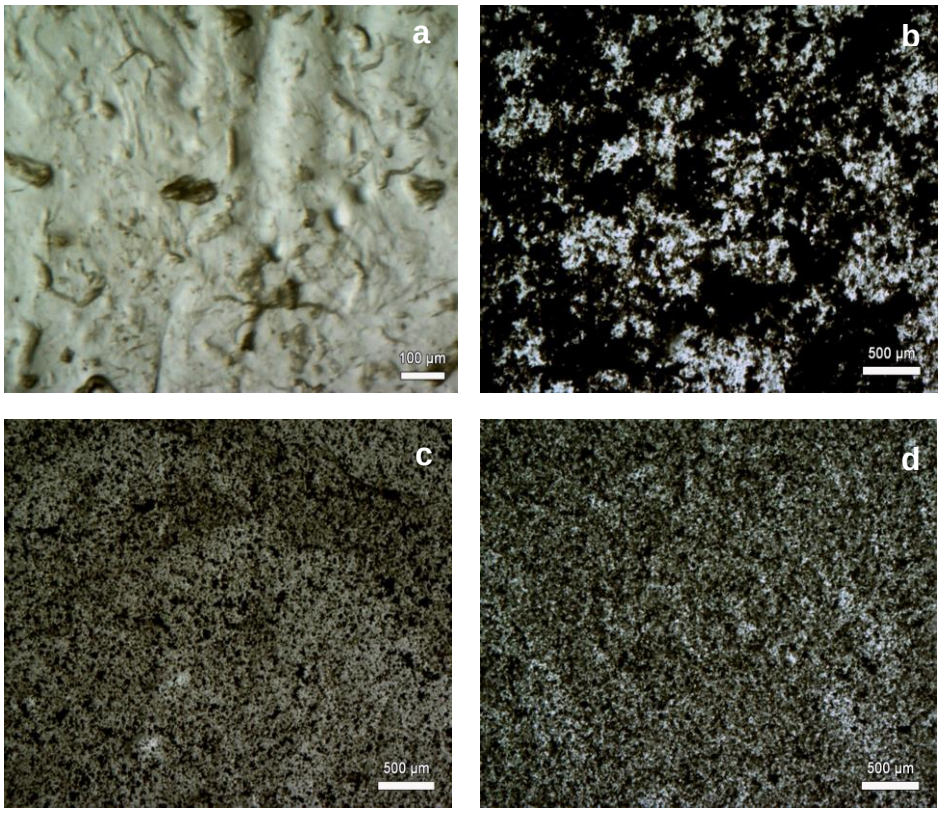

Figure 19. Optical micrographs of the films a) HCl b) AA c) CNT d) Ch.

4.3 Fourier Transform Infrared Spectroscopy

The effects of the insertion of CNT to the polymeric matrix structure (Figure 20) were studied. Figure 21 shows the FTIR spectrum of the bare chitin sample and the three chitin-CNT composites. All four samples produced similar spectra. The characteristic peak of chitin due to carbonyl vibration modes of the amide I between 1600 and 1620 cm^{-1} is apparent. This band splits into two, at 1651 cm^{-1} due to the hydrogen bonds between

the carbonyl and amino groups of the same chain and at 1624 cm^{-1} due to the same hydrogen bond and an additional the hydrogen bonds between chains. These crosslinks are responsible for the chemical stability of the polymer. The presence of the split signal demonstrates that the matrix is the allomorph α-chitin [38][39]. Vibrations of C—N are visible at 1554 cm^{-1}. Furthermore, OH and NH vibrations bands are at 3421 and 3263 cm^{-1}, respectively. The first one can be attributed to intramolecular hydrogen bonds between the hydroxyl and the oxygen, while the second one represents the intermolecular hydrogen bonds to the amide vibrations [38][40].

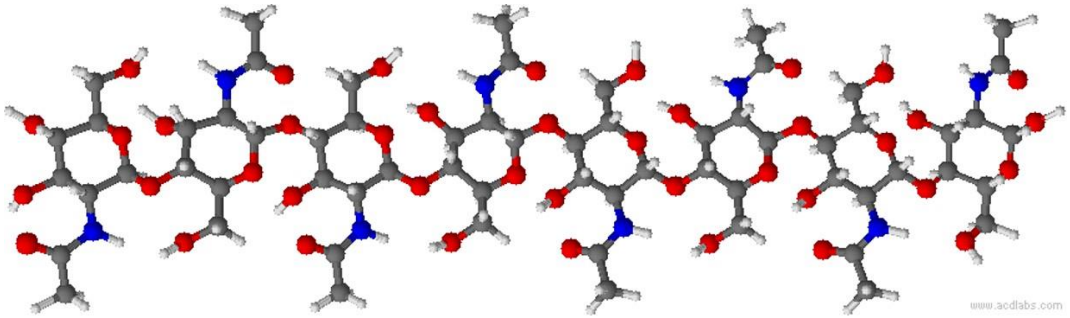

Chitin

Figure 20. Chitin polymeric chain.

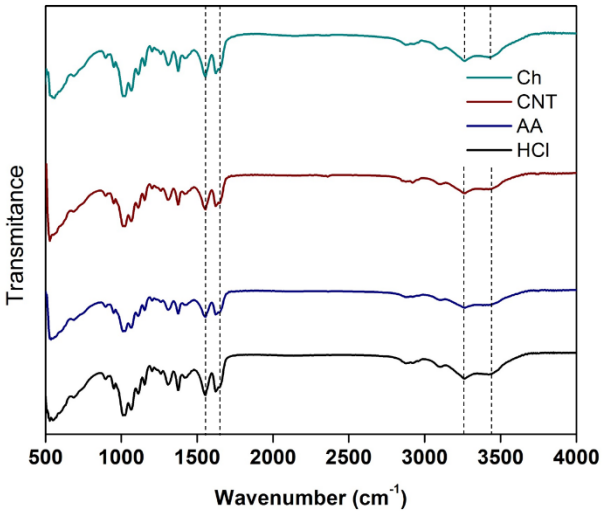

Figure 21. FT-IR spectra for bare chitin and the three chitin-CNT composites.

4.4 Thermogravimetric Analysis (TGA)

The effect of addition of CNT dispersion into the matrix on the degradation temperature was also investigated. The TGA plots are shown in Figure 23 and Figure 24. In Figure 23 we can observe the mass loss of all four specimens as the temperature increases. A first smooth step indicating the mass loss of volatile and/or solvent residues can be observed from 40 to 125°C. About 6 to 9% of the samples weight is water or solvent residues. The addition of the CNT did not affect the water retention of the films. The degradation of the four different composites starts approximately at 225°C. Figure 22 shows the thermal degradation curve corresponding to bare chitin powder where degradation temperature of 275°C was registered. Also, one can observe that the bare chitin powder contained around 5wt.% moisture. This is 1 to 4% less than the composite.

The higher amount of moisture in the composites can be due to the increase of free volume space of the chain created during the process of fabrication compared with the bare chitin powder. Moreover, this moisture can be a product of the solvent used in the synthesis of the composites. The degradation temperature values for the Ch-CNTs composite films did not displayed significant variations for the different films tested. The first derivative revealed that the point of steepest weight loss rate is at 269°C (Figure 24).

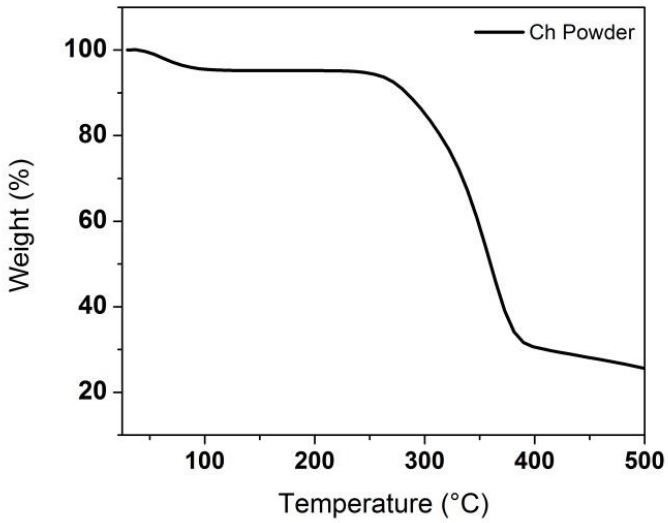

Figure 22. Weight loss percent versus sample temperature of chitin powder.

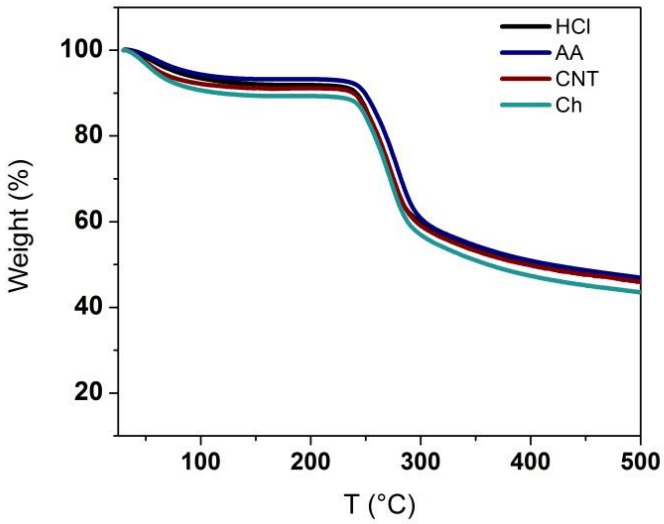

Figure 23. Weight loss percent versus sample temperature.

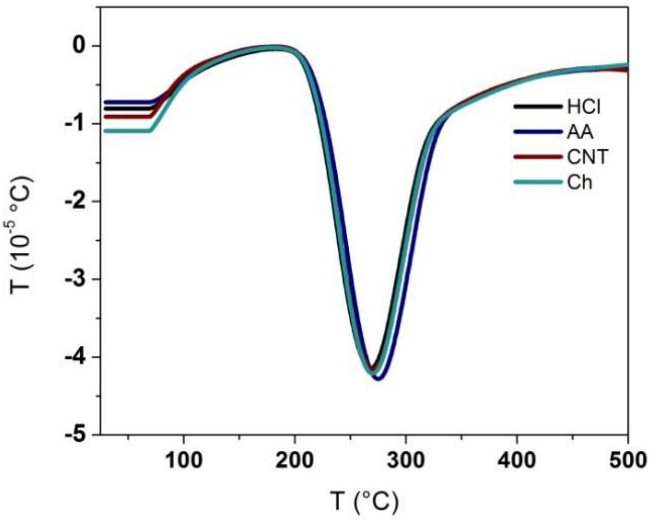

Figure 24. First derivative of TGA curves.

4.5 Glass Transition Temperature and Coefficient of Thermal Expansion

The SDTA results showed in Figure 25 evinced a smooth endothermic signal around 50ºC followed of a constant heat liberation. This signal could be due to water evaporation similar to the ones observed in the DSC thermograms from the first chitin-CNT composites mentioned in the section 4.1. Also, by comparing the thermal behavior of the chitin films with the other three composites no significant changes are apparent. These measurements did not suffice to measure the T_g. Figure 26 displays how using the deformation vs. temperature curve, the onset point is calculated from the slope change which then can be attributed to the glass transition (Figure 9). Thus, the T_g values were estimated and the results for the bare chitin and the chitin-CNTs films did not manifest significant variations for the different films tested, as one can see in Figure 27. Besides the glass transition the deformation around 200ºC of the samples was determined and the results are summarized in Figure 28. These results reflect the CNT reinforcement effect on the chitin. As expected, the average deformation values were higher for the bare chitin films than the composites. The higher dispersion observed in the chitin films can be seen also for the T_g values. The lower dispersions of the composites could be due to an increase of the molecular packing of the polymer reducing the movement of chitin chains.

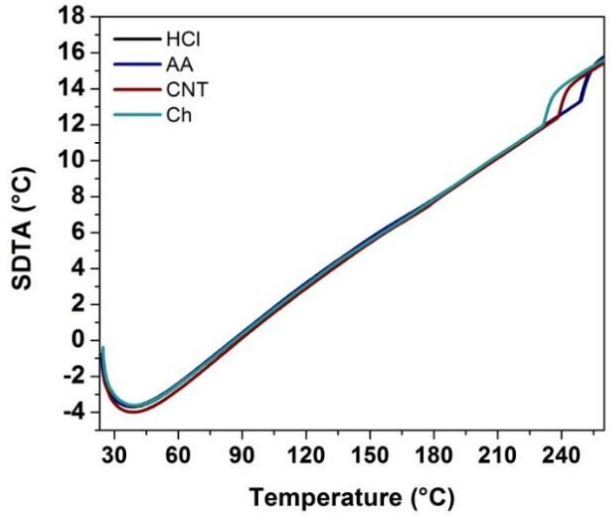

Figure 25. Temperature change versus sample temperature of the chitin and chitin-CNT composites.

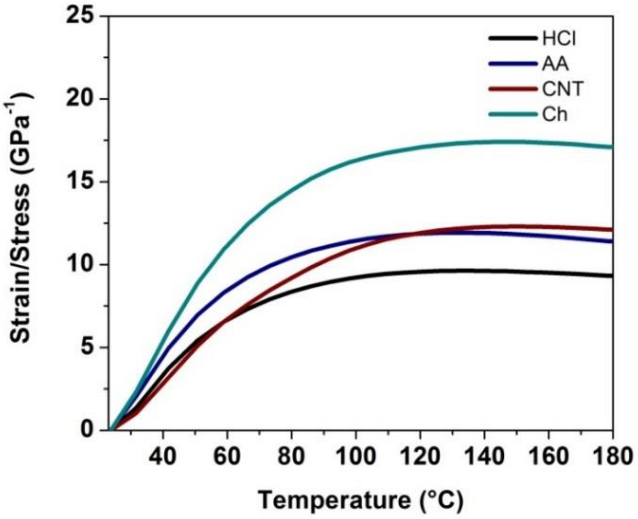

Figure 26. Deformation as a function of temperature of the chitin and chitin-CNT composites.

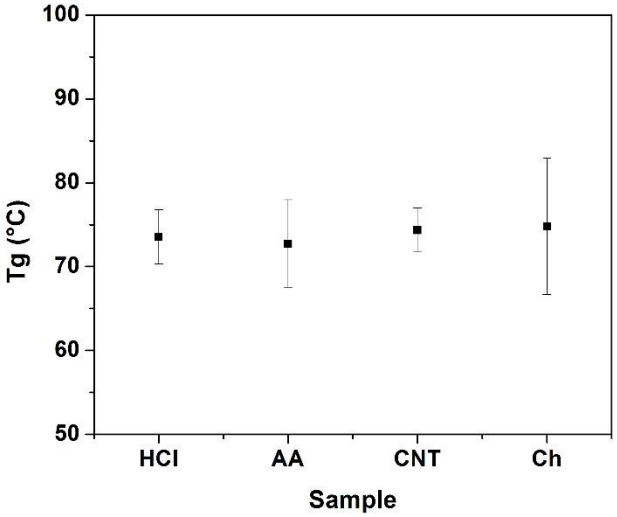

Figure 27. Glass transitions values for Ch, HCl, AA and CNT samples.

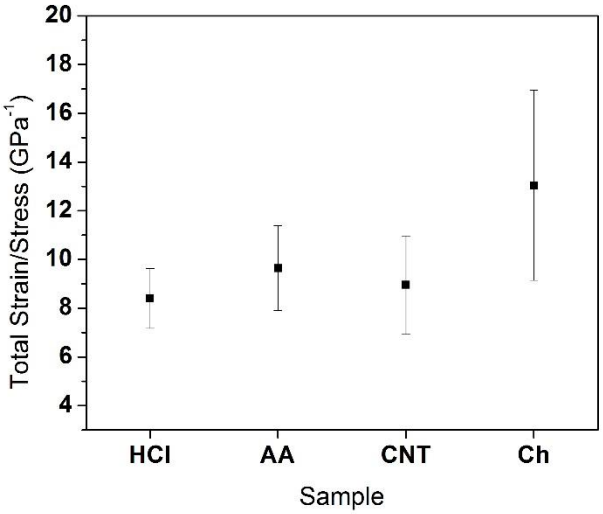

Figure 28. Total strain values at 200ºC for Ch, HCl, AA and CNT samples.

The CTE values were obtained from 75 to 200ºC. For the composites the values were from 3.5 5.3x10^{-5}/ºC and 2.7x10^{-5}/ºC for the matrix (Figure 29). The higher values of CTE were obtained from the samples with CNT, one reason for this increase can be due to the good thermal conduction of the CNT. The other two samples containing CNT

did not show a significant increase in the CTE. This could be due to damaged CNTs walls resulting from the acid treatments. These results are similar to CTE values obtained from XRD measurements (Table 3). These values are also similar to the values of CTE found for chitin nanofibers poly(vinyl alcohol) composites [19] and the chitin found in the Morpho butterfly wing [41], 2.5 and 2.2x10^{-5}/ºC respectively.

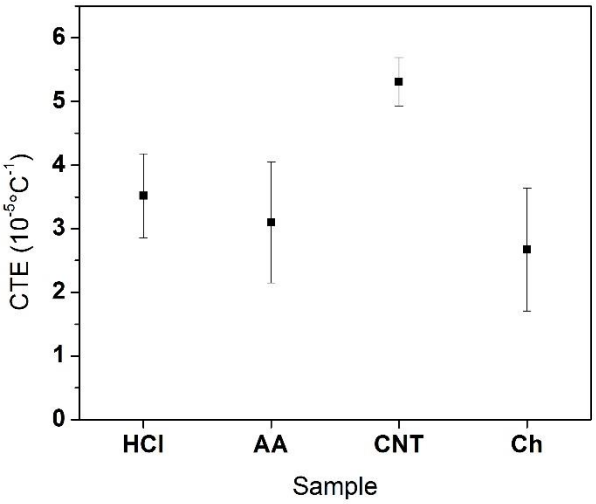

Figure 29. Coefficient of thermal expansion for Ch, HCl, AA and CNT samples.

Sample	CTE (10^{-5}/ºC)
HCl	4.09
AA	2.90
CNT	4.93
Ch	4.51

Table 3. CTE values calculated from XRD data.

4.6 Creep

The TMA allowed completing creep experiments at four different temperatures and at a constant load of 0.5N. For the extension of time studied, the curves obtained showed a decreasing strain rate (first creep stage) followed by a constant strain rate (second creep stage). In general and as expected, the creep strain for all samples increased with temperature. Raising temperature from 25º to 150ºC increased the creep compliance from 2.35 to 14.38, at t =3h. Figure 33 shows creep compliance curves for the bare chitin and the chitin films reinforced with carbon nanotubes at 150ºC. As expected, higher values of deformation were obtained for the bare chitin films. Conversely, the films containing CNTs treated with acetic acid had the smallest deformation at 150ºC (Figure 33). One can observe that the creep deformation at any given time decreased remarkably with the addition of MWCNT to the matrix; this is particularly so at 150ºC. Additionally, at room temperature the composite films without treated CNT showed less deformation than the other three samples (Figure 30). After averaging the values for creep compliance at a given time, we found that there was no significant difference between the four different samples at room temperature. This finding implies that the creep behavior is improved by the presence of nanotubes only at temperatures around 150ºC.

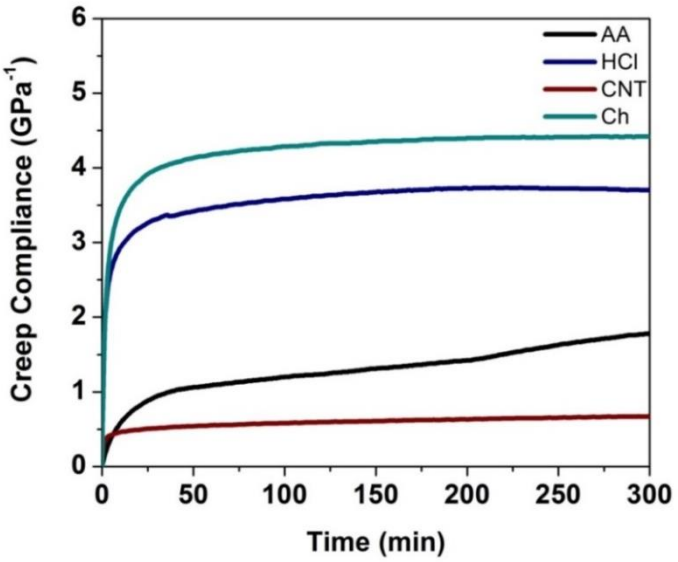

Figure 30 Creep compliance versus time at constant load of 0.5N and 25°C.

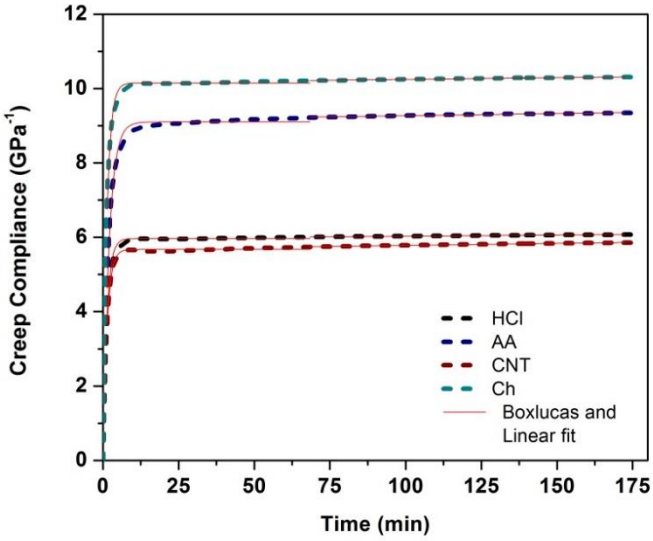

Figure 31. Creep compliance versus time at a constant load of 0.5N and at 75°C.

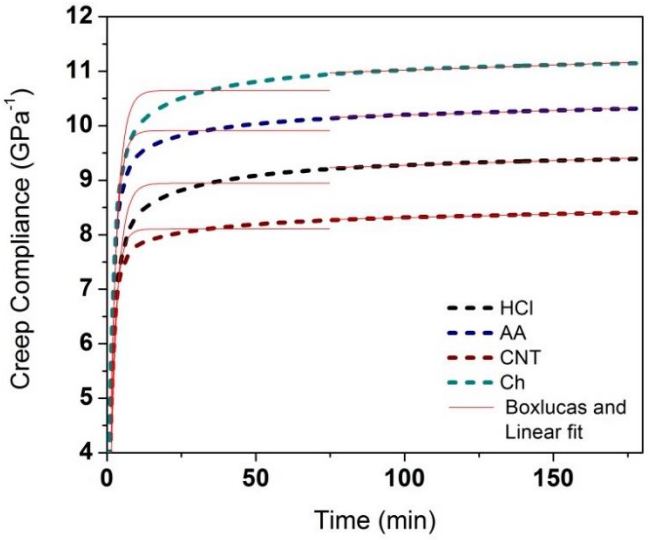

Figure 32. Creep compliance versus time at a constant load of 0.5N and at 100°C.

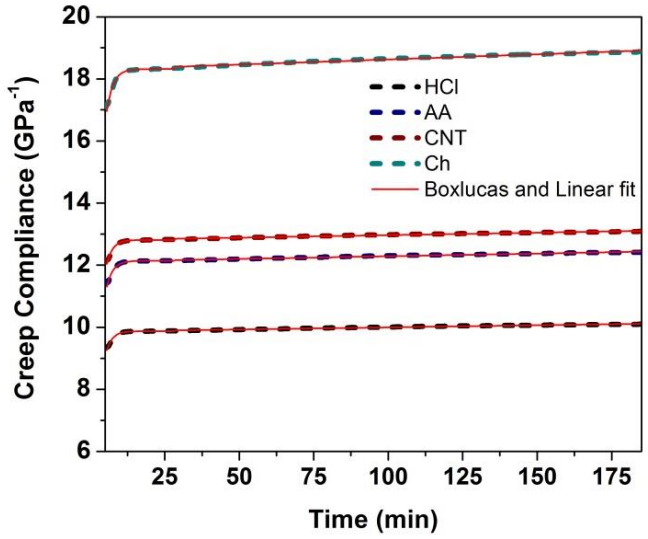

Figure 33. Creep compliance versus time at a constant load of 0.5N and at 150°C.

For each creep curve, we computed a Box-Lucas and a linear regression model with the form: $y = a(1 - e^{-bx})$ and $y = mx + b$ respectively [42]. Using these two regressions, the coefficients $E_1, E_2, \eta_1,$ and η_2 in equation 6 were calculated (Table 4 to

Table 6). The E_1 and E_2 coefficients represent the elastic recovery and the rubbery elasticity of the composites, respectively.

At 150ºC the E_1 values for the bare chitin films were lower than the values obtained for the three other films containing CNTs. In other words, the instantaneous deformation is higher for the films without nanotubes. This means that the nanocomposites suffered less deformation upon loading at a given temperature. This strain is independent of time and will disappear (full recovery) once the load is removed. Furthermore, the values of E_2 for the bare chitin films were lower than the values calculated for the composites. This increase in E_2 for the films with the CNT represents an improvement of the material stiffness associated to the amorphous part of the semicrystalline polymer. Both coefficients are related to the elasticity and stiffness of the material: The higher the values of E the lower the elastic deformation will be. For our composite it is believed that the CNTs are restraining the chain relative movement in terms of uncoiling and bond rotations. The values of η_1 were higher for the nanocomposites, i.e. lower values of permanent creep strain. This is attributed to the presence of CNTs that can reduce the slip between the matrix polymer chains and, thus, lowering the permanent deformation of the composite. Finally, the fourth parameter, i.e. η_2, was higher for the nanocomposites, indicating that the CNTs likely helped lower the steady state creep strain associated with the viscous flow of the chains. We believe that there is a decrease in chain mobility that translates in a smaller permanent deformation of the material. In summary, the highest values of modulus (E_1 and E_2) were measured in the films with CNT. For them the viscosity coefficient from the Maxwell model (η_1) is significantly higher than the coefficient from the

Voigt model (η_2). These viscosity coefficients represent the molecular slip and delayed elasticity [18]. These translates into lower elastic and permanent deformation for the composites. As stated before, the registered improvement of the creep behavior of the composite was observed at temperatures above 100°C. We suspect that at 100°C and below the mobility of the polymer chains is lower than the mobility of the CNT within the matrix allowing the deformation to occur. In other words the matrix creep deformation was reduced only at the rubbery state of the polymer. During the rubbery state of the matrix the CNTs could be entering in the free volume space of the polymer, reducing remarkably its deformation.

In general, the Burgers model appears to closely match the experimental results of creep tests conducted in the TMA.

$$J = \frac{1}{E_1} + \frac{1}{E_2}\left[1 - exp\left(-\frac{E_2 t}{\eta_2}\right)\right] + \frac{t}{\eta_1} \quad 6$$

Sample	Burger coefficient (75°C)			
	E_1	E_2	η_1	η_2
HCl	0.15	0.15	1272.2	0.23
AA	0.10	0.10	861.78	0.17
CNT	0.14	0.14	799.64	0.19
Ch	0.11	0.11	957.98	0.17

Table 4. Burger coefficients at 75°C

Sample	Burger coefficient (100°C)			
	E_1	E_2	η_1	η_2
HCl	0.14	0.14	1091.43	0.25
AA	0.09	0.09	644.75	0.15
CNT	0.13	0.13	857.91	0.23
Ch	0.11	0.11	887.87	0.23

Table 5. Burger coefficients at 100°C

Sample	Burger coefficient (150°C)			
	E_1	E_2	η_1	η_2
HCl	0.11	0.11	713.29	0.25
AA	0.11	0.11	692.36	0.26
CNT	0.10	0.10	705.42	0.21
Ch	0.07	0.07	552.85	0.16

Table 6. Burger coefficients at 150°C

An alternative approach to analyze the creep behavior is using the power law presented in equation 7. Plots of the decimal log of creep compliance vs the decimal log of time are shown in Figure 34 to Figure 36. A linear regression analysis permitted to compute the mean creep compliance strain rate n, as presented in Table 7. Evidently, the composites with CNTs deformed at a slower pace as compared to the bare chitin samples. As discussed before, this behavior was only observed in the creep experiments at 150°C.

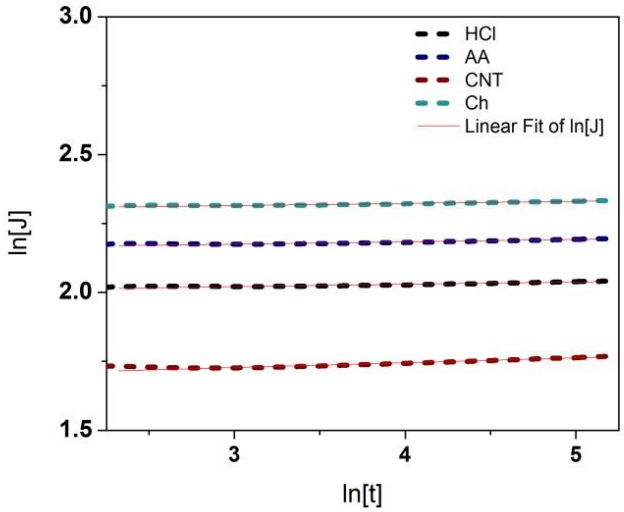

Figure 34. Linear regression for ln(J) vs ln(t) at a constant load of 0.5N and at room temperature (75ºC)

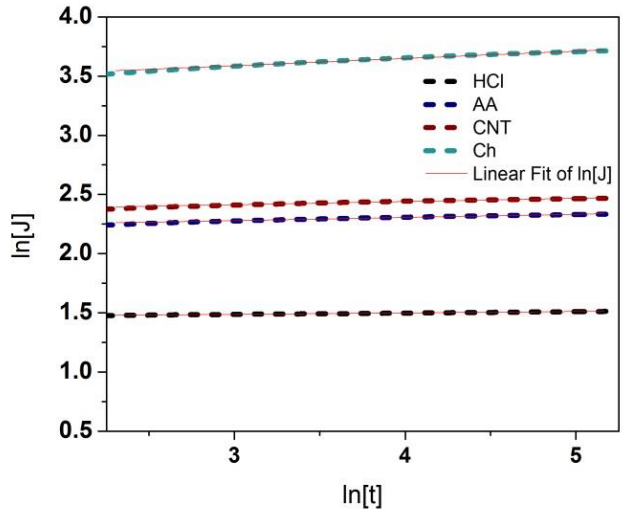

Figure 35. Linear regression for ln(J) vs ln(t) at a constant load of 0.5N and at room temperature (100ºC).

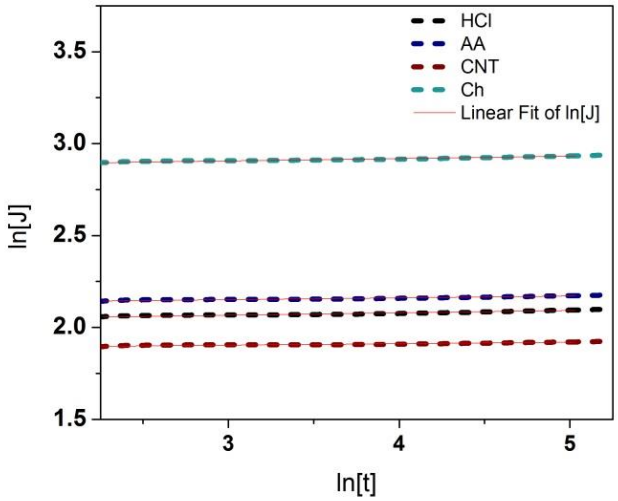

Figure 36. Linear regression for ln(J) vs ln(t) at a constant load of 0.5N and at 150ºC.

Sample	n (150°C, 3h)	n (100°C, 3h)	n (75°C, 3h)
AA	$1.94x10^{-2}$	$1.00X10^{-2}$	$1.09X10^{-2}$
HCl	$1.88X10^{-2}$	$7.29X10^{-3}$	$1.18X10^{-2}$
CNT	$2.13X10^{-2}$	$1.06X10^{-2}$	$1.33X10^{-2}$
Ch	$3.62X10^{-2}$	$9.57X10^{-3}$	$1.53X10^{-2}$

Table 7. Values of creep compliance rate for the chitin and chitin-CNT films.

Sample	J (150°C, 3h)	J (100°C, 3h)	J (75°C, 3h)
AA	8.91	9.72	8.59
HCl	7.04	4.02	6.67
CNT	5.98	4.71	5.40
Ch	17.3	16.1	9.10

Table 8. Values of creep compliance constant J_1 for the chitin and chitin-CNT films.

In general, comparing Figure 30 to Figure 33, one can corroborate that increasing the temperature results in larger total creep strains in the composites. Also, at high temperatures the reinforcing effect of the CNT in the matrix can be observed. Furthermore, the creep curves showed that the secondary stage was initiated approximately after 75 minutes for most samples.

5. Conclusions

Bare chitin films were successfully synthetized. Shrinkage of the film was reduced by using cold press as drying method. CNT were successfully incorporated and dispersed into the matrix. Through FT-IR we determined that the addition of CNT to the polymeric matrix did not affect its structure. The degradation temperature for chitin and the composites was 270ºC. Also, the water amount was determined using TGA and was about 6% for chitin and the composites. The T_g of the composites was not affected by the addition of CNT: 73ºC for the composites and the bare chitin films. The creep behavior of the chitin and the chitin-CNT was analyzed at 150ºC, 100ºC and 75ºC and followed the Burgers model. When the strain rate of the films was calculated using the power law, the results revealed that films made with the CNTs had more resistance to creep at 150ºC. At that same temperature, the composites showed a significant reduction in strain rate compared to the bare chitin films. However, at 100ºC and 75ºC the films made with CNT did not exhibited any evident increase in creep resistance or lower strain rates in comparison with the chitin films. These results suggested that the reinforcement becomes effective only at high temperature, i.e. 150ºC. It is believe that since att this temperature the polymer is in its rubbery state, i.e. above its glass transition temperature, this results in the CNTs entering in the free volume space restraining the movement.

6. References

[1] S. Duan, L. Li, Z. Zhuang, W. Wu, S. Hong, and J. Zhou, “Improved production of chitin from shrimp waste by fermentation with epiphytic lactic acid bacteria,” *Carbohydr. Polym.*, vol. 89, no. 4, pp. 1283–1288, Aug. 2012.

[2] J. D. Kittle, C. Wang, C. Qian, Y. Zhang, M. Zhang, M. Roman, J. R. Morris, R. B. Moore, A. R. Esker, K. Aoi, and A. Takasu, “Ultrathin chitin films for nanocomposites and biosensors.,” *Biomacromolecules*, vol. 13, no. 3, pp. 714–8, Mar. 2012.

[3] M. Rinaudo, “Chitin and chitosan: Properties and applications,” *Prog. Polym. Sci.*, vol. 31, no. 7, pp. 603–632, Jul. 2006.

[4] Y. X. Xu, K. M. Kim, M. a. Hanna, and D. Nag, “Chitosan–starch composite film: preparation and characterization,” *Ind. Crops Prod.*, vol. 21, no. 2, pp. 185–192, Mar. 2005.

[5] Y. Liu, L. Yu, S. Zhang, J. Yuan, L. Shi, and L. Zheng, “Dispersion of multiwalled carbon nanotubes by ionic liquid-type Gemini imidazolium surfactants in aqueous solution,” *Colloids Surfaces A Physicochem. Eng. Asp.*, vol. 359, no. 1–3, pp. 66–70, Apr. 2010.

[6] M. Peng-Cheng and K. Jang-Kyo, “Application of CNT/Polymer Nanocomposites,” in *Carbon Nanotubes for Polymer Reinforcement*, CRC Press, 2011, pp. 169–191.

[7] B. P. Grady, “Mechanical and Rheological Properties,” in *Carbon Nanotube–Polymer Composites*, John Wiley & Sons, Inc., 2011, pp. 191–247.

[8] B. P. Grady, “Dispersion, Orientation, and Lengths of Carbon Nanotubes in Polymers,” in *Carbon Nanotube–Polymer Composites*, John Wiley & Sons, Inc., 2011, pp. 59–117.

[9] M. A. Salam, M. S. I. Makki, and M. Y. a. Abdelaal, “Preparation and characterization of multi-walled carbon nanotubes/chitosan nanocomposite and its application for the removal of heavy metals from aqueous solution,” *J. Alloys Compd.*, vol. 509, no. 5, pp. 2582–2587, Feb. 2011.

[10] A. Sharma, B. Tripathi, and Y. K. Vijay, “Dramatic Improvement in properties of magnetically aligned CNT/polymer nanocomposites,” *J. Memb. Sci.*, vol. 361, no. 1–2, pp. 89–95, Sep. 2010.

[11] B. Munkhbayar, M. J. Nine, J. Jeoun, M. Bat-Erdene, H. Chung, and H. Jeong, “Influence of dry and wet ball milling on dispersion characteristics of the multi-walled

carbon nanotubes in aqueous solution with and without surfactant," *Powder Technol.*, vol. 234, pp. 132–140, Jan. 2013.

[12] K. Jang-Kyo, "CNT/Polymer Nanocomposites," in *Carbon Nanotubes for Polymer Reinforcement*, CRC Press, 2011, pp. 115–167.

[13] K. Jang-Kyo, "CNT/Polymer Nanocomposites," in *Carbon Nanotubes for Polymer Reinforcement*, CRC Press, 2011, pp. 115–167.

[14] E. T. Thostenson and T.-W. Chou, "Processing-structure-multi-functional property relationship in carbon nanotube/epoxy composites," *Carbon N. Y.*, vol. 44, no. 14, pp. 3022–3029, Nov. 2006.

[15] L. Carson, C. Kelly-Brown, M. Stewart, A. Oki, G. Regisford, Z. Luo, and V. I. Bakhmutov, "Synthesis and characterization of chitosan-carbon nanotube composites.," *Mater. Lett.*, vol. 63, no. 6–7, pp. 617–620, Mar. 2009.

[16] M. C. Gortari and R. A. Hours, "Biotechnological processes for chitin recovery out of crustacean waste: A mini-review," *Electron. J. Biotechnol.*, vol. 16, no. 3, May 2013.

[17] N. Thirunavukkarasu, K. Dhinamala, and R. Moses Inbaraj, "Production of chitin from two marine stomatopods," *J. Chem. Pharm. Res.*, vol. 3, no. 1, pp. 353–359, 2011.

[18] P. M. Visakh, M. Monti, D. Puglia, M. Rallini, C. Santulli, F. Sarasini, S. Thomas, and J. M. Kenny, "Mechanical and thermal properties of crab chitin reinforced carboxylated SBR composites," vol. 6, no. 5, pp. 396–409, 2012.

[19] Q. Deng, J. Li, J. Yang, and D. Li, "Optical and flexible α-chitin nanofibers reinforced poly(vinyl alcohol) (PVA) composite film: Fabrication and property," *Compos. Part A Appl. Sci. Manuf.*, vol. 67, pp. 55–60, 2014.

[20] B. P. Grady, "Carbon Nanotubes," in *Carbon Nanotube–Polymer Composites*, John Wiley & Sons, Inc., 2011, pp. 11–57.

[21] M. F. L. De Volder, S. H. Tawfick, R. H. Baughman, and a J. Hart, "Carbon nanotubes: present and future commercial applications.," *Science*, vol. 339, no. 6119, pp. 535–9, Feb. 2013.

[22] J. N. Coleman, U. Khan, W. J. Blau, and Y. K. Gun'ko, "Small but strong: A review of the mechanical properties of carbon nanotube–polymer composites," *Carbon N. Y.*, vol. 44, no. 9, pp. 1624–1652, Aug. 2006.

[23] R. Andrews and M. . Weisenberger, "Carbon nanotube polymer composites," *Curr. Opin. Solid State Mater. Sci.*, vol. 8, no. 1, pp. 31–37, Jan. 2004.

[24] J. B. González-Campos, G. Luna-Bárcenas, D. G. Zárate-Triviño, A. Mendoza-Galván, E. Prokhorov, F. Villaseñor-Ortega, and I. C. Sanchez, “Polymer States and Properties,” in *Handbook of Polymer Synthesis, Characterization, and Processing*, John Wiley & Sons, Inc., 2013, pp. 15–39.

[25] H. Ribeiro, W. Silva, M.-T. Rodrigues, J. Neves, R. Paniago, C. Fantini, H. R. Calado, L. Seara, and G. Silva, “Glass transition improvement in epoxy/graphene composites,” *J. Mater. Sci.*, vol. 48, no. 22, pp. 7883–7892, 2013.

[26] D. R. Riesen and D. J. Schawe, “The glass transition temperature measured by different TA techniques. Part 1: Overview,” *UserCom*. METTLER TOLEDO, pp. 1–20, Jan-2003.

[27] “Thermal Properties of Polymers,” *Polymers and Liquid Crystals*. [Online]. Available: http://plc.cwru.edu/tutorial/enhanced/files/polymers/therm/therm.htm. [Accessed: 03-May-2014].

[28] B. P. Grady, “Effects of Carbon Nanotubes on Polymer Physics,” in *Carbon Nanotube–Polymer Composites*, John Wiley & Sons, Inc., 2011, pp. 119–189.

[29] Y. Rao and T. N. Blanton, “Polymer Nanocomposites with a Low Thermal Expansion Coefficient,” *Society*, pp. 935–941, 2008.

[30] “Thermal Diffusivity and Coefficient of Thermal Expansion of Composites,” in *Electromagnetic, Mechanical, and Transport Properties of Composite Materials*, CRC Press, 2014, pp. 295–302.

[31] S. Houshyar, R. a. Shanks, and a. Hodzic, “Tensile creep behaviour of polypropylene fibre reinforced polypropylene composites,” *Polym. Test.*, vol. 24, no. 2, pp. 257–264, Apr. 2005.

[32] “Overview of Crystal/Defect Structure and Mechanical Properties and Behavior,” in *Mechanical Properties of Engineered Materials*, CRC Press, 2002.

[33] W. Soboyejo, “Introduction to Viscoelasticity, Creep, and Creep Crack Growth,” in *Mechanical Properties of Engineered Materials*, CRC Press, 2002.

[34] W. N. Findley and K. Onaran, *Creep and Relaxation of Nonlinear Viscoelastic Materials: With an Introduction to Linear Viscoelasticity*. Dover Publications, Incorporated, 1976.

[35] A. J. Nuñez, N. E. Marcovich, M. I. Aranguren, U. Nacional, and D. Mar, “Analysis of the Creep Behavior of Polypropylene-Woodflour Composites,” vol. 44, no. 8, 2004.

[36] E. M. El-Nesr, A. I. Raafat, S. M. Nasef, E. A. Soliman, and E.-S. A. Hegazy, “Chitin and Chitosan Extracted from Irradiated and non-Irradiated Shrimp Wastes (Comparative Analysis Study),” *Arab J. Nucl. Sci. Appl.*, vol. 46, no. 1, pp. 53–66, 2013.

[37] “Agilent Nano Indenter G200 Data Sheet.” pp. 1–4, 2013.

[38] M. Rinaudo, “Chitin and chitosan: Properties and applications,” *Prog. Polym. Sci.*, vol. 31, no. 7, pp. 603–632, Jul. 2006.

[39] J. Kumirska, M. Czerwicka, Z. Kaczyński, A. Bychowska, K. Brzozowski, J. Thöming, and P. Stepnowski, “Application of spectroscopic methods for structural analysis of chitin and chitosan.,” *Mar. Drugs*, vol. 8, no. 5, pp. 1567–636, Jan. 2010.

[40] Serkan KELESGLU, “COMPARATIVE ADSORPTION STUDIE S OF HEAVY METAL IONS ON CHITIN AND CHITOSAN BIOPOLYMERS,” Engineering and Science of Izmir Institute of Technology, 2007.

[41] S. Niu, B. Li, Z. Mu, M. Yang, J. Zhang, Z. Han, and L. Ren, “Excellent Structure-Based Multifunction of Morpho Butterfly Wings: A Review,” *J. Bionic Eng.*, vol. 12, no. 2, pp. 170–189, 2015.

[42] M. Kallumadil, M. Tada, T. Nakagawa, M. Abe, P. Southern, and Q. A. Pankhurst, “Suitability of commercial colloids for magnetic hyperthermia,” vol. 321, pp. 1509–1513, 2009.

APPENDICES

A. **Chitin Cellulose Composites**

Chitin-carbon nanotubes (Ch-CNT) composites in form of films were successfully fabricated. The fabrication of the films consisted of the coagulation of chitin from a solution form. Then CNT and acid treated CNT were incorporated in the chitin solution. The Ch-CNT composites were strong but brittle which can limit their applications. In order to increase the flexibility of the films cellulose was added to the matrix. To fabricate the chitin-cellulose-CNT (Ch-Cell-CNT) new composites (**Error! Reference source not ound.**), cellulose was added to the chitin solution (9:1 chitin to cellulose) and the procedure describe in sections 3.2 to 3.4 was followed.

Table 1 The four different samples prepared for the characterization.

Sample	Description
HCl	Chitin-cellulose films with CNT treated using HCl and HNO_3.
AA	Chitin-cellulose films with CNT treated using acetic acid.
CNT	Chitin-cellulose films with CNT as bough from Sigma Aldrich.
Ch-Cell	Bare chitin-cellulose films.

Glass transition and thermal stability of the new composites were studied using DTA, TMA and TGA techniques. The effects of the insertion of CNT to the matrix on the degradation temperature were explored. The TGA thermograms are shown in Figure 37. In this Figure 37 we can observe the mass loss of the four different specimens containing cellulose and one of a bare chitin film as the temperature increases. A first smooth step

indicating the mass loss of volatile and/or solvent residues can be observed from 40 to 125°C. About 10% of the samples weight is water or solvent residues. Degradation of the four different composites containing cellulose starts at 220°C. Similar to the Ch-CNT composites the addition of CNT to the Ch-Cell matrix did not affect their thermal stability. By comparing these results with the Ch-CNT composites we can observe a decrease in the degradation temperature when cellulose is added to the matrix. The Ch-CNT films starts to degrade at 240°C. Also one can observe that the Ch-Cell-CNT had around 10w% moisture. This is 3% more than the Ch-CNT composites. The higher amount of moisture in the composites can be due to the increase of free volume space of the chain compared to the bare chitin composites. Moreover, this moisture can be a product of the solvent used in the preparation of the composites. The degradation temperature values for the Ch-Cell-CNTs films do not evidence significant variations in the different films tested. The first derivative reveals the point of steepest rate of change on the weight loss curve is at 235°C Figure 38.

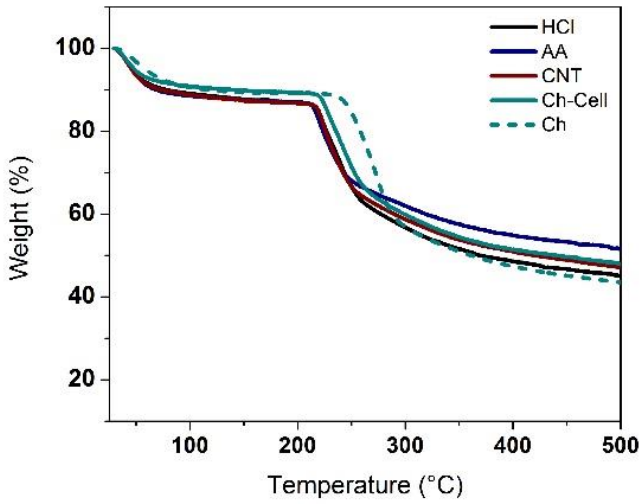

Figure 37. TGA curves for the four different specimens.

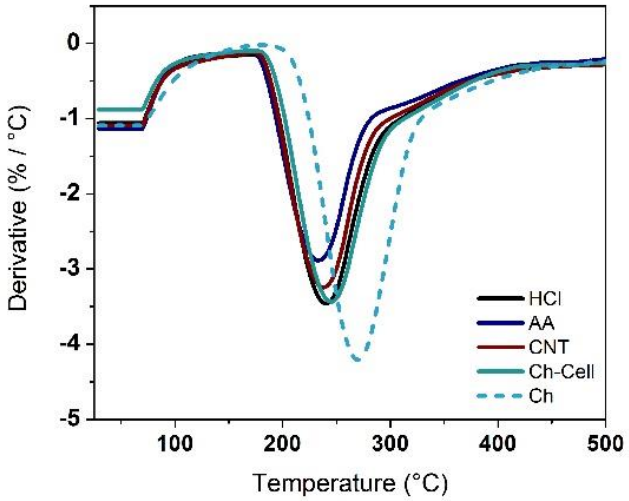

Figure 38 . TGA first derivative curves for the four different specimens.

The TMA/SDTA 841e allowed completing creep experiments at 150°C and at a constant load of 0.5N. The creep resistance of the films decreased with the addition of cellulose to the matrix in comparison with the results obtained for Ch-CNT. This could be caused by weak interaction between the two polymers. Also the interaction of cellulose with the CNT may be weaker than the interaction of the CNT with a chitin matrix. In the creep curves obtained, the secondary creep stage initiated approximately after 120 min for most samples. Higher values of deformation were obtained for the CNT films. Conversely, the films made with the carbon nanotubes functionalized with acetic acid had the smallest deformation at 150ºC. Figure 39 shows an example of the creep behavior of the Ch-Cell composites.

Besides the creep behavior, the TMA was used to evaluate the glass transition temperature (T_g). The T_g values for the Ch-Cell-CNTs films varied from 69 to 93 ºC, calculated from the change of slope in the curves showed in Figure 40. These results higher variability than the values obtained from the Ch composites. For the Ch-CNT films the T_g values were found to be between 72 and 75 ºC. In these curves a larger deformation of the CNT was observed, which is in agreement with the results obtained at a constant temperature of 150ºC.

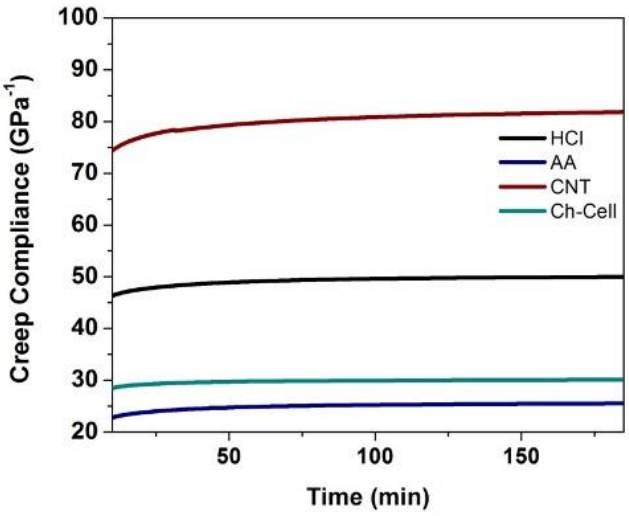

Figure 39. Creep curves for Ch-Cell-CNT composites.

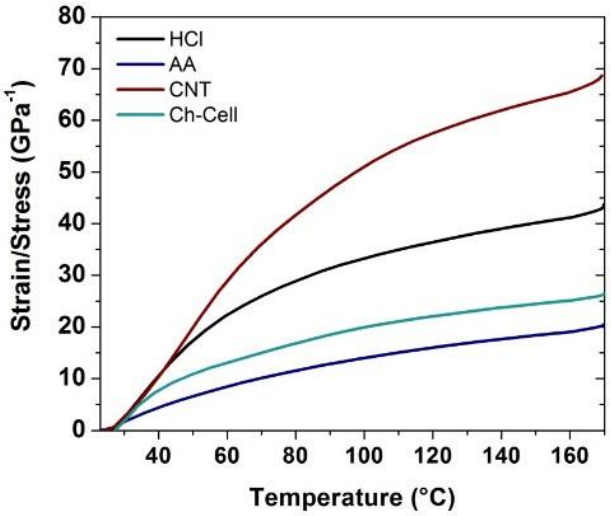

Figure 40. Strain versus temperature of the Ch-Cell-CNT composites.

So far this composite had showed more elasticity in comparison with the ones fabricated using a matrix of bare chitin. But by adding elasticity the matrix is less resistant.